Chemical Physics Impact 7 (2023) 100323

Contents lists available at ScienceDirect

Chemical Physics Impact

journal homepage: www.sciencedirect.com/journal/chemical-physics-impact

Fluorescence property and solvent effect on *m*-bromosalicylaldehyde derivative; insights from synthesis, characterization, antimicrobial activity and computational studies

C. Geetha Priya [a], B.R. Venkatraman [a], S. Sowrirajan [b], N. Elangovan [b,*], Natarajan Arumugam [c], Abdulrahman I. Almansour [c], Sakkarapalayam M. Mahalingam [d]

[a] Department of Chemistry, Thanthai Periyar Government Arts and Science College (Autonomous), Affiliated to Bharathidasan University, Tiruchirappalli-620023, Tamilnadu, India
[b] Research Centre for Computational and Theoretical Chemistry, Anjalam-621208, Musiri, Tiruchirappalli, Tamilnadu, India
[c] Department of Chemistry, College of Science, King Saud University, P.O. Box 2455, Riyadh 11451, Saudi Arabia
[d] Department of Chemistry, 720 Clinic Drive, Purdue University, West Lafayette, IN 47907, USA

ARTICLE INFO

Keywords:
Solvation study
DFT
Fluorescence
Molecular docking
Non-covalent interaction

ABSTRACT

The Schiff base was synthesized using the *m*-bromosalicylaldehyde and ethylenediamine in 1:1 mole ratio. Using the infrared, UV, fluorescence and ^{1}H-^{13}CNMR spectral analysis the *m*-bromosalicylaldehyde derivative structure was confirmed. Using DFT study the compound structure was optimized. Local energy decomposition (LED) analysis calculated binding energy is -9.19 kcal/mol. The molecule 5BRSET is a optical material, its wavelength is 512 nm and 784 nm respectively. We used three different solvents to calculate the non-linear optical, HOMO-LUMO and molecular electrostatic potential studies, when compared to other solvent the water is showed good activity. Using topological analysis we confirms the localization and delocalization electrons from the synthesized compound. The non-covalent interaction study confirms the intermolecular and intermolecular hydrogen bondings. The natural bond orbital analysis calculation showed the interactions between and within the molecule. A docking study was done on the molecule, and the results show that 5BRSET interacts well with the crystal structure of hypothetical protein (PDB ID: 2EA9). The molecule is moderate activity, which is confirmed by antimicrobial activity.

Introduction

The Schiff base was made when combination of amine with aldehyde or ketone. Schiff bases are formed through the condensation reaction between primary amines and carbonyl compounds [1]. In biological function the Schiff base such as -CH═N- (imine) group is the very important role [2]. In a Schiff base molecule, an alkyl or aryl group is linked to a nitrogen atom. The azomethine compound play identical significant character in pharmacological activity, because present in nitrogen atom [3]. The pharmacological properties of this substance contain antibacterial, antifungal, antiviral, antihelmintic, anticonvulsant, antitumor, anti-inflammatory, anti-HIV, anticancer, antimalarial, antitubercular, and corrosion-inhibiting activities. The formation of Schiff bases was shown to arise from the reaction between ethylenediamine and 5-bromosalicylaldehyde [4]. DNA is the most important drug target for anticancer drugs.

In addition to their use in the clinical setting, Schiff base complexes also find use in the analytical sector. In oxygen transport systems, some Schiff bases model cellular oxygen carrier molecules. It is common knowledge that tetradentate Schiff bases can combine to create stable complexes, and the mechanism through which this coordination occurs is the N_2O_2 donor set. Transition metal ions complexed with polydentate Schiff bases containing nitrogen and oxygen donor atoms play a crucial role in biological processes. These complexes also serve as intriguing models for metalloenzymes involved in the reduction of dinitrogen and dioxygen. Biological systems feature transition metal ion-polydentate Schiff base complexes with nitrogen and oxygen donor atoms. Anisha Bharduraj et.al, recently reported the organotellurium (IV) complex derived from Schiff base ligand [5]. In this study reported the various characterization, antimicrobial, antioxidant, DFT, docking and ADMET

* Corresponding author.
E-mail address: drelangovanchem@gmail.com (N. Elangovan).

https://doi.org/10.1016/j.chphi.2023.100323
Received 18 August 2023; Received in revised form 15 September 2023; Accepted 25 September 2023
Available online 26 September 2023

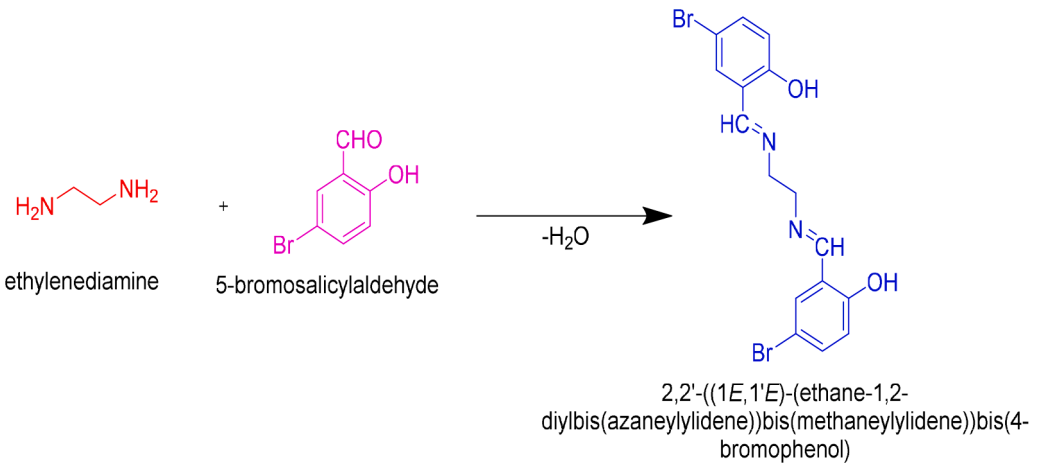

Fig. 1. Synthesis of 2,2′-((1E,1′E)-(ethane-1,2-diylbis(azaneylylidene)) bis (methaneylylidene)) bis(4-bromophenol) (5BRSET).

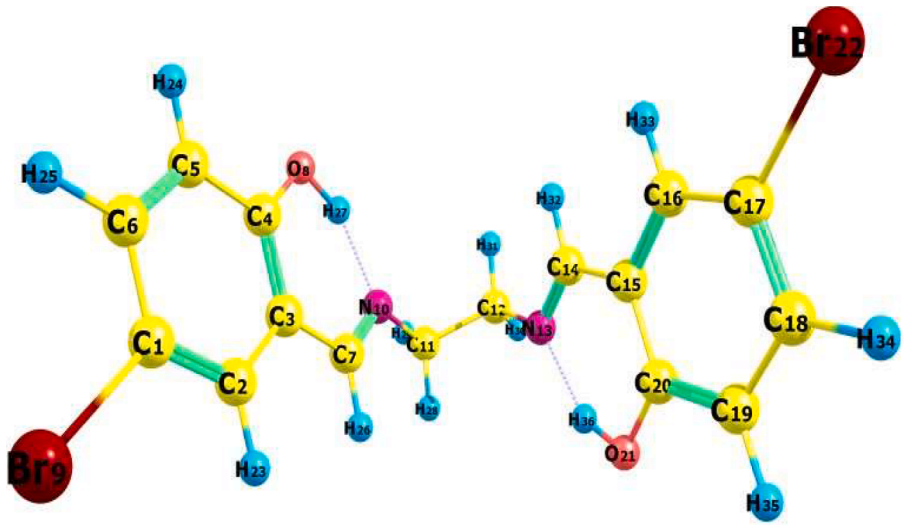

Fig. 2. Optimized structure of 2,2′-((1E,1′E)-(ethane-1,2-diylbis(azaneylylidene)) bis (methaneylylidene)) bis(4-bromophenol).

Table 1
Local energy decomposition (LED) energy studies of 2,2′-((1E,1′E)-(ethane-1,2-diylbis (azaneylylidene)) bis (methaneylylidene)) bis(4-bromophenol) with water.

Formula	Energy (kcal/mol)
$E_{int} = E^{opt}_{dimer} - E^{opt}_{monomer}$	−9.19
$DE_{geo\text{-}prep} = E^{fixed}_{monomer} - E^{opt}_{monomer}$	1.11
$DE^{C\text{-}(T)}_{int} = E^{C\text{-}(T)}_{dimer} - E^{C\text{-}(T)}_{water\text{-}fixed} - E^{C\text{-}(T)}_{carbene\text{-}fixed}$	−0.08
$DE^{ref}_{el\text{-}prep} = E^{ref}_{intra} - E_{X\text{-}fixed}$	30.01
$DE^{C\text{-}CCSD}_{no\text{-}disp} = E^{C\text{-}CCSD}_{no\text{-}disp} - E_{Corr\text{-}X} - E_{Corr\text{-}Y}$	−2.74
$DE = DE_{geo\text{-}prep} + DE^{ref}_{el\text{-}prep} + E^{ref}_{elstat} + E^{ref}_{exch} + DE^{C\text{-}CCSD}_{no\text{-}disp} + E^{C\text{-}CCSD}_{disp} + DE^{C\text{-}(T)}_{int}$	−9.19

properties. The Mamtra et.al, reported the in *vitro* cytotoxicity of manganese (II) Schiff base metal complex, in cytotoxicity study the used *HeLa* and *MCF7* cell lines [6]. Mst. Sabina Begum et.al, recently studied synthesis and characterization of Ni (II) Schiff base complex, including antimicrobial and DFT studies [7]. Kalarani et.al, recently studied the antimicrobial and DNA binding studies on Co (II), Cu (II) and Zn (II) metal complexes [8]. Shehnaz et.al synthesis a Cu (II) and Zn (II) metal complexes derived from sulphonamide Schiff base [9].

In this paper we focus to synthesis a new Schiff base. The experimental characterization studies compared by the simulated characterization studies. Electrophilic and nucleophilic attacking sites confirmed using MEP studies. In solvation study we used DLPNO–CCSD (T) auxiliary basis set. The titled compound antimicrobial activity tested against *S. aureus, S. pneumoniae* and *E. coli* and *candida albicans*. The docking study also done using autodock software.

Experimental

Materials and instrumentation

5-bromosalicylaldehyde and ethylenediamine both purchased from Sigma Aldrich. Solvents are purchased at local chemical shops and it is used directly. The range between 4000 and 400 cm^{-1} the infrared spectrum were recorded, using KBr pellet model. Using Burker Avance-400 MHZ FT-NMR spectrophotometer the NMR was recorded in chloroform solvent. Using LS-45 spectrophotometer and Perkin Elmer Lambda-35 spectrophotometer, the fluorescence and Uv-Visible spectra were recorded.

Synthesis of 2,2′-((1E,1′E)-(ethane-1,2-diylbis(azaneylylidene))bis (methaneylylidene))bis(4-bromophenol) (5BRSET)

The 5-bromosalicylaldehyde (4.02 mg, 0.02 mm) and ethylenediamine (6 ml, 0.02 mm) were mixed. The above reaction mixture was

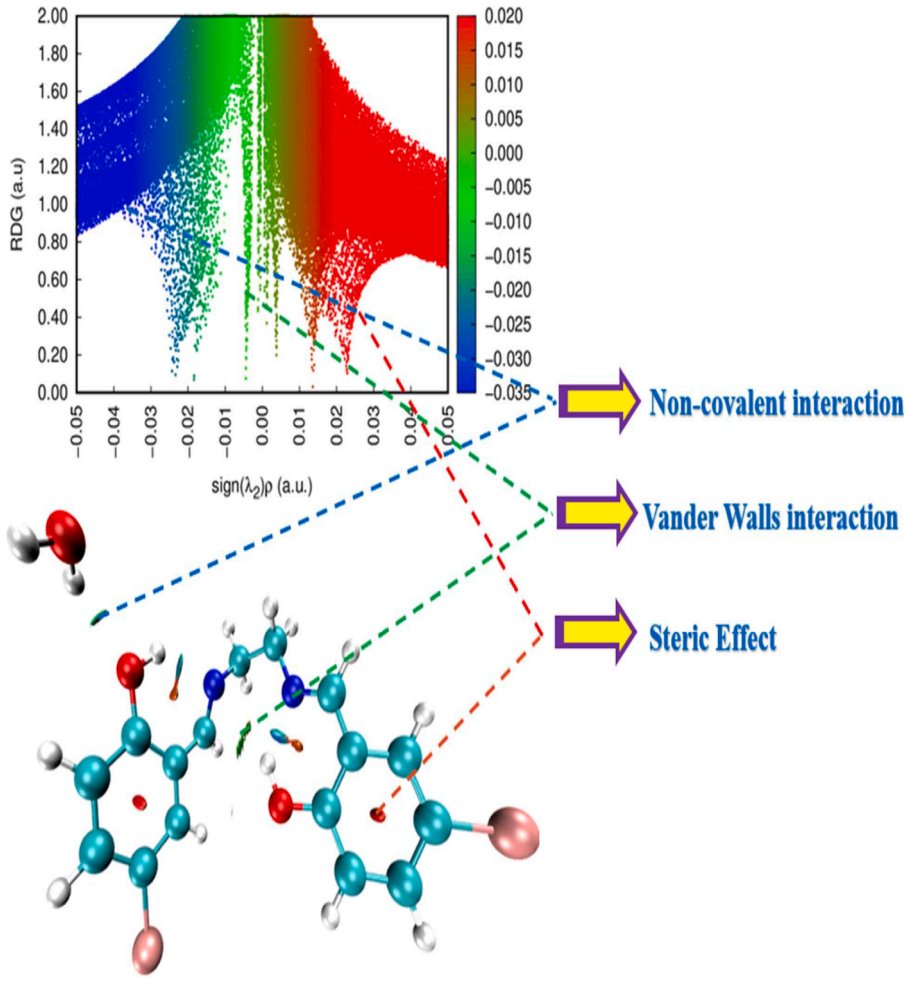

Fig. 3. Non-covalent interaction of 2,2′-((1E,1′E)-(ethane-1,2-diylbis(azaneylylidene)) bis (methaneylylidene)) bis(4-bromophenol) with water complex.

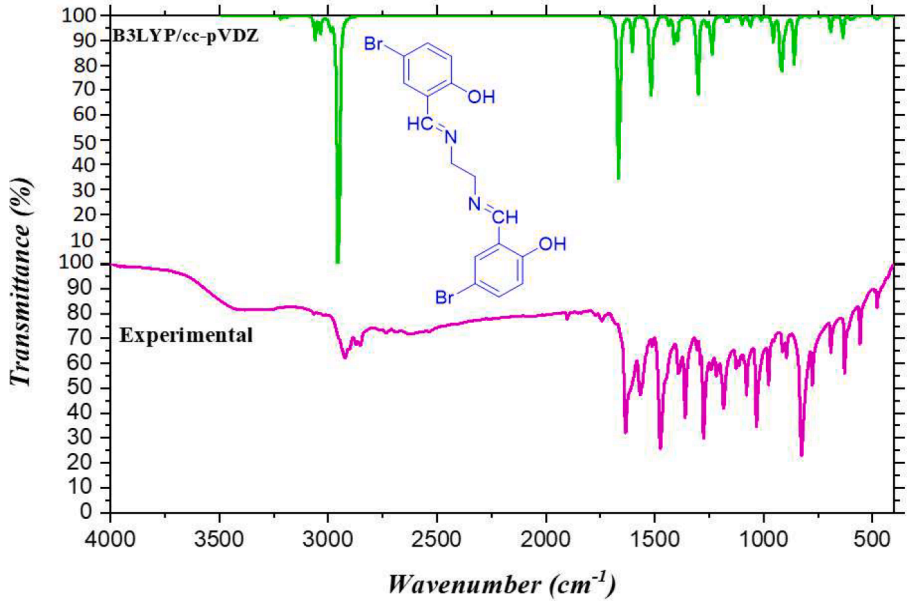

Fig. 4. FTIR spectrum (experimental and calculated) of 2,2′-((1E,1′E)-(ethane-1,2-diylbis(azaneylylidene)) bis (methaneylylidene)) bis(4-bromophenol).

Table 2
FTIR spectral analysis and PED analysis of 2,2′-((1E,1′E)-(ethane-1,2-diylbis(azaneylylidene)) bis (methaneylylidene)) bis(4-bromophenol).

B3LYP/cc-pVDZ					Observed	
Mode	**Unscaled**	**Scaled**	**IR_I**	**R_A**	**IR**	**Assignment (% PED)**
102	3217.84	3105.54	1.1672	292.71		CH(98)
101	3217.83	3105.53	10.441	49.652		CH(98)
100	3200.42	3088.73	0.9923	78.919		CH(97)
99	3200.41	3088.72	0.7703	37		CH(97)
98	3188.89	3077.6	5.4146	0.9144	3064	CH(98)
97	3188.86	3077.57	0.3316	64.879		CH(98)
96	3061.96	2955.1	42.157	500.27		CH(93)
95	3059.98	2953.19	21.166	64.159		CH(78)
94	3037.41	2931.4	43.77	6.2116		CH(99)
93	3036.48	2930.51	0.3762	106.21	2923	CH(99)
92	2992.37	2887.94	23.233	22.764		CH(74)
91	2986.79	2882.55	13.693	280.2	2872	CH(99)
90	2956.47	2853.29	432.51	53.613	2852	OH(93)
89	2950.91	2847.92	514.96	41.529		OH(93)
88	1668.32	1610.1	229.72	444.77		CC(58)
87	1665.46	1607.34	171.09	302.08		CC(60)
86	1661.05	1603.08	83.68	41.357	1634	NC(52)+HOC(11)
85	1659.48	1601.56	46.796	73.329		NC(44)+HOC(10)
84	1604.33	1548.34	22.102	53.717	1567	CC(47)+HOC(16)
83	1603.79	1547.82	59.681	41.997	1512	CNC(12)+OC(14)+HOC(14)
82	1525.79	1472.54	33.92	23.302	1475	HCH(66)+HCNC(15)
81	1520.17	1467.12	136.69	17.672		HCH(75)
80	1514.94	1462.07	96.916	2.973		HOC(17)+HCC(33)
79	1513.14	1460.33	35.03	20.193		HOC(12)+HCC(24)+HCH(14)
78	1496.33	1444.11	17.828	159.83		OC(12)+HOC(23)
77	1495.79	1443.59	10.644	200.13		HOC(10)
76	1436.93	1386.78	6.7273	8.2315	1391	CC(16)+HOC(11)+HCC(11)+HCN(26)
75	1434.8	1384.73	14.948	4.6427		CC(23)+HOC(13)+HCC(12)+HCN(24)
74	1410.79	1361.55	53.631	32.795	1361	CC(10)+HCH(10)+HCNC(41)
73	1407.52	1358.4	29.537	35.733		CC(12)+HCC(11)+HCN(15)+HCNC(18)
72	1396.16	1347.43	49.984	9.4827		CC(11)+HCN(35)+HCNC(11)
71	1380.39	1332.21	5.1043	31.681		HCN(23)+HCH10+HCNC(43)
70	1355.07	1307.78	2.7613	46.849	1305	CC(67)
69	1354.68	1307.4	1.0612	79.586		CC(15)
68	1303.25	1257.77	116.78	2.1265	1291	CC(34)+HCC(13)+HCN(11)
67	1302.73	1257.26	162.84	0.4124		OC(25)+HCC(12)
66	1290.84	1245.79	1.1269	50.355		HCN(48)+HCNC(12)
65	1287.43	1242.5	2.0623	5.3507	1240	CC(10)+OC(16)+HCN(43)
64	1277.02	1232.45	1.0012	82.338		CC(21)+HCC(22)
63	1262.33	1218.27	26.144	53.109	1217	HCN(51)
62	1240.9	1197.59	40.81	42.387		CC(46)+HCC(10)
61	1237.52	1194.33	83.436	29.642	1184	CC(53)+HCC(13)
60	1170.05	1129.22	13.004	3.5997		CC(18)+HCC(29)
59	1164.65	1124	10.841	1.6471	1114	CC(16)
58	1136.42	1096.76	5.0752	0.3457	1079	CC(10)+HCN(17)+HCNC(23)
57	1098.27	1059.94	17.913	5.59		CC(49)+HCN(10)+HCC(10)
56	1096.63	1058.36	7.7148	13.551		CC(29)+HCC(12)+HCC(14)
55	1065.32	1028.14	14.478	0.1531	1033	NC(25)+HCC(30)+CCN(12)+HCNC(26)
54	1060.34	1023.33	20.346	55.505		CC(71)
53	1012.31	976.98	8.5834	1.2086	978	NC(20)+HCNC(49)
52	1011.28	975.986	2.0743	12.44		HCNC(62)
51	997.38	962.571	0.6344	0.0488		HCCC(72)+CCCC(11)
50	996.84	962.05	0.1768	0.9267	952	HCCC(64)
49	957.39	923.977	66.421	0.1785	913	NC(10)+CCC(19)+HCNC(30)
48	923.05	890.836	68.324	4.4289	895	HCCC(39)
47	921.75	889.581	5.9961	0.5786		HCCC(69)
46	920.21	888.095	0.002	12.815		CCC(19)
45	919.45	887.361	68.403	1.6953		HOCC(37)+HCCC(25)
44	916.2	884.225	64.396	0.1981		HOCC(85
43	904.62	873.049	57.396	3.0366		HOCC(44)
42	889.37	858.331	10.067	3.8926		CC(53)+HCNC(17)
41	858.87	828.895	30.731	1.3931		HCCC(76)
40	858.65	828.683	93.443	0.6231	825	HCCC(74)
39	790.75	763.153	6.6577	6.1118	776	CC(17)+OC(14)+CCC(24)
38	789.41	761.86	0.0188	38.395		OC(32)+CCC(26)
37	738.14	712.379	2.481	0.1892		HCCC(10)+CCCC(14)+OCCC(46)
36	737.7	711.954	1.5321	1.129	691	CCCC(42)
35	692.34	668.177	21.08	0.3142		CCC(31)
34	690.88	666.768	18.544	2.0176		CC(10)+CCC(21)
33	638.21	615.936	40.707	0.0446	628	BrC(14)+CCC(39)
32	636.05	613.852	21.118	3.0322		OC(14)+BrC(18)+CCC(38)
31	600.39	579.436	14.637	0.1386		CCN(10)+CCCC(39)
30	588.02	567.498	6.1161	0.4407	557	CCCC(36)

(*continued on next page*)

Table 2 (*continued*)

B3LYP/cc-pVDZ					Observed	
Mode	**Unscaled**	**Scaled**	**IR_I**	**R_A**	**IR**	**Assignment (% PED)**
29	553.47	534.154	2.8268	0.8848		CCN(34)
28	486.72	469.733	3.3842	0.6153	489	CCN(11)+CCO(23)+CCCC(19)
27	483.02	466.163	0.1624	2.0117		CCN(10)+CCO(66)+CCCC(14)
26	482.58	465.738	3.8148	1.0626	478	CCCC(10)
25	473.84	457.303	9.0173	1.6388		CCO(10)+CCCC(16)
24	451	435.26	0.0023	2.2316		CCN(22)+CCO(16)
23	402.33	388.289	3.2652	5.1275		CCC(44)
22	378.3	365.097	4.0239	2.5299		CCN(16)
21	367.26	354.443	7.1229	0.2378		CC(10)+CCC(37)
20	357.96	345.467	0.6754	2.0713		CCCC(50)
19	356.97	344.512	2.4683	0.0609		OCCC(19)
18	338.68	326.86	0.0649	4.9949		CCN(30)
17	285.14	275.189	1.2858	0.3235		CCCC(56)
16	282.68	272.814	16.725	0.0938		CCCC(67)
15	269.91	260.49	3.5764	6.5485		BrC(57)+CCC(11)
14	268.81	259.429	3.4993	9.086		BrC(48)+CCBr(12)
13	249.01	240.32	4.8153	1.8954		CCC(10)+CCN(37)
12	230.25	222.214	0.4537	1.1366		CCBr(64)
11	173.39	167.339	1.1177	5.1995		CCCC(33)
10	172.57	166.547	0.4735	0.478		CCBr(45)+CCCC912)
9	130.4	125.849	4.0294	1.9412		CCBr(79)
8	122.88	118.591	1.7923	3.5561		CCCC(45)
7	111.81	107.908	3.9813	0.4561		CCCC(72)
6	92.5	89.2718	0.116	7.4066		CCCC(53)
5	63.22	61.0136	0.2289	1.3859		CCC(37)+CCN(14)
4	59.4	57.3269	0.0076	3.5604		CCCC(71)
3	16.55	15.9724	0.1613	8.4939		NCCN(77)
2	10.08	9.72821	0.8253	3.7669		CCCC(11)+CCCN(73)
1	7.04	6.7943	0.0031	3.9335		CCN(10)+CCCC(16)+CNCC(64)

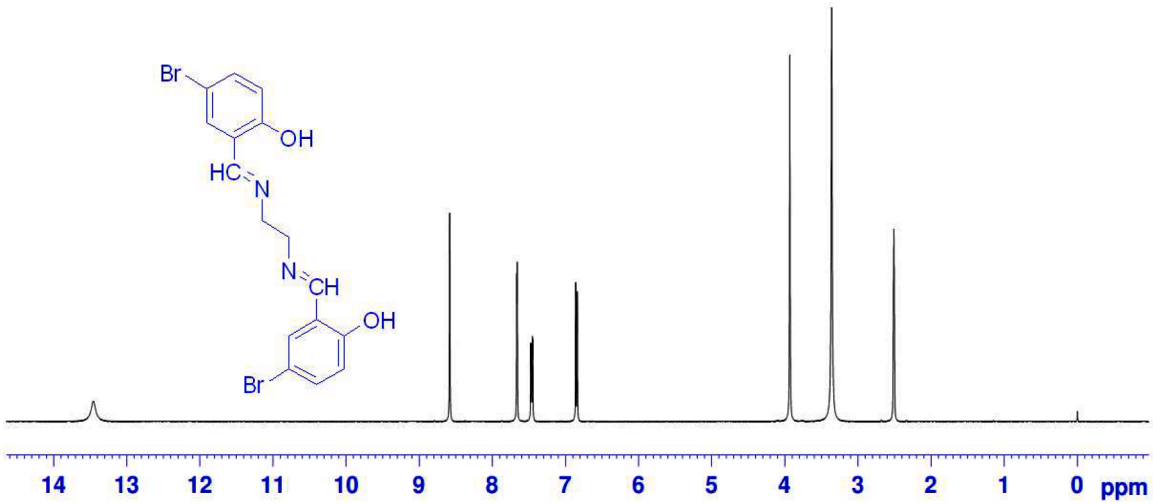

Fig. 5. ^{1}HNMR spectra of 2,2′-((1E,1′E)-(ethane-1,2-diylbis(azaneylylidene)) bis (methaneylylidene)) bis(4-bromophenol).

transferred in to RB flask, using methonal (25 ml) the mixture was stirred 5 h in water bath. After completed reaction the reaction mixture is filtered and washed in methanol and recrystalled in chloroform [10, 11]. The final product 5BRSET dried and stored in vacuum desiccator. The scheme of the reaction we presented in Fig. 1.

Antimicrobial action

The antibacterial activity of the synthesised compound 5BRSET was assessed using the disc diffusion method. The antibacterial activity was assessed against gram-negative bacterium *E. coli* and gram-positive bacteria Staphylococcus aureus and Streptococcus pneumoniae, respectively [12]. We take a 5BRSET molecule that was 1 mg/ml and mixed it with DMSO solvent. After 24 h, the inhibition zone (mm) was used to measure the area of inhibition. Amoxicillin was used as a positive control [13]. Antifungal activity was tested against 5BRSET compound using potato dextrose agar diffusion method. We used *candida albicans* microorganism [14]. Initially, the test strain was inoculated into a culture medium known as potato dextrose broth (PDB) and incubated at a temperature of 30 °C. The plates were kept at 30 °C and in the light for 24 h.

Computational methods

The titled compound structure was optimized with Gaussian software, and optimized structure was visualized in Gauss View-6 [15]. In LED study using ORCA software the interaction energy were calculated using DLPNO–CCSD(T) auxiliary basis set [16,17]. The VEDA programme was employed for the examination of the analysis of PED [18]. The TD-DFT method used for figure out the simulated UV–Visible

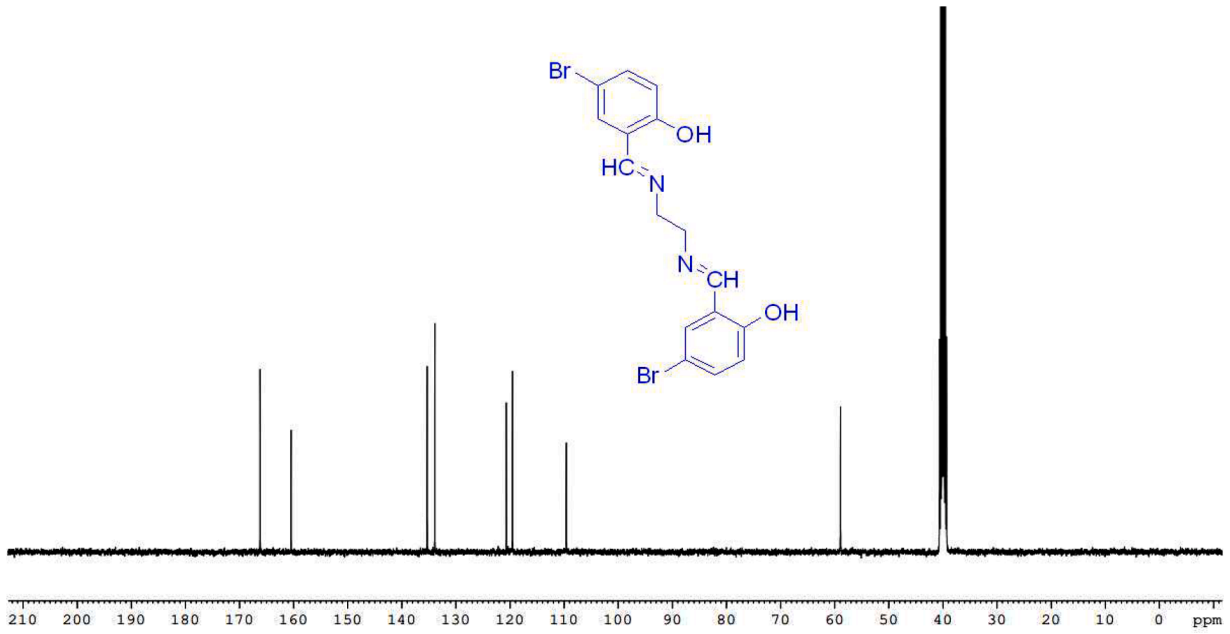

Fig. 6. ^{13}CNMR spectra of 2,2′-((1E,1′E)-(ethane-1,2-diylbis(azaneylylidene)) bis (methaneylylidene)) bis(4-bromophenol).

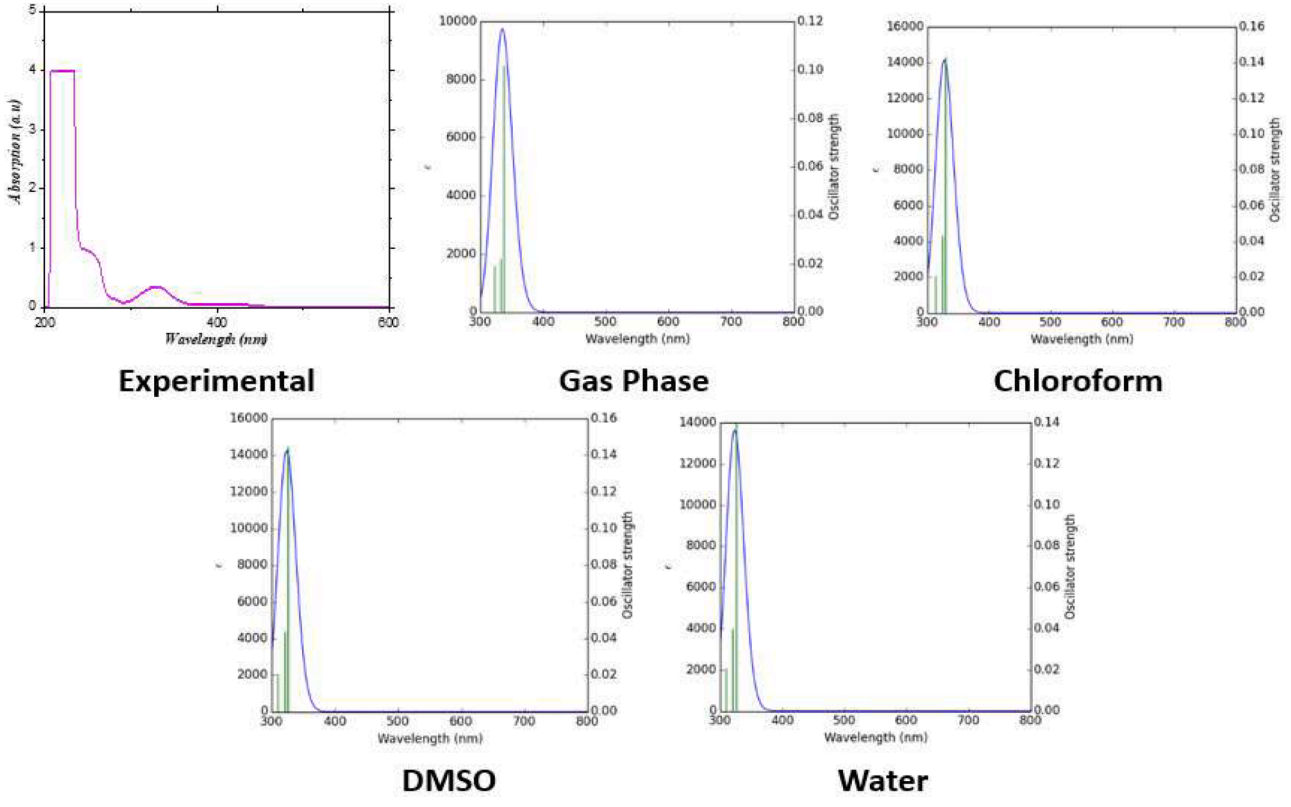

Fig. 7. UV–Visible spectrum of 2,2′-((1E,1′E)-(ethane-1,2-diylbis(azaneylylidene)) bis (methaneylylidene)) bis(4-bromophenol).

spectrum using IEFPCM solvation model and different types of solvents like chloroform, DMSO, water and gas phase [19]. The general GIAO method was used to find out the simulated ^{1}HNMR and ^{13}CNMR spectra, both are calculate from chloroform solvent [20]. The Multiwfn programme is used to find out quantum chemistry-related LOL, ELF, and RDG studies [21]. The docking was done using autodock software with X, Y, Z centres are 60 × 60 × 60, with grid size is 1.0. Before docking the protein was prepared using discovery studio visualizer. We used genetic alothrium, we do four docking studies each docking studies we set 10 confirmations.

Results and discussions

Structural analysis

Vconf software was used for the conformational analysis, after

Table 3
Electronic transitions of 2,2′-((1E,1′E)-(ethane-1,2-diylbis(azaneylylidene)) bis (methaneylylidene)) bis(4-bromophenol) with gas phase and different solvents.

Media	Wavelength (nm)	Band Gap eV	Energy (cm-1)	Oscillator strength	Contribution
	391.3			0.056	
Experiment	329.45			0.354	
	220.55			4	
	337.7648313		29,606.39792	0.1019	HOMO->LUMO (94 %), H-1->*L* + 1 (4 %)
Gas	332.6179387		30,064.524	0.0222	H-1->LUMO (95 %), HOMO->*L* + 1 (2 %)
	322.3109071		31,025.94352	0.019	HOMO->*L* + 1 (95 %), H-1->LUMO (3 %)
	330.1380286		30,290.3608	0.1432	HOMO->LUMO (91 %), H-1->*L* + 1 (7 %)
Chloroform	324.691205		30,798.4936	0.0435	H-1->LUMO (88 %), HOMO->*L* + 1 (8 %)
	313.6674593		31,880.89712	0.0208	H-1->LUMO (10 %), HOMO->*L* + 1 (89 %)
	326.443751		30,633.1488	0.1447	HOMO->LUMO (91 %), H-1->*L* + 1 (7 %)
DMSO	320.8927625		31,163.05872	0.0436	H-1->LUMO (87 %), HOMO->*L* + 1 (9 %)
	310.2453185		32,232.55728	0.021	H-1->LUMO (10 %), HOMO->*L* + 1 (88 %)
	325.9202877		30,682.34896	0.1395	HOMO->LUMO (91 %), H-1->*L* + 1 (6 %)
Water	320.3538232		31,215.48512	0.0401	H-1->LUMO (88 %), HOMO->*L* + 1 (8 %)
	309.9738403		32,260.78688	0.0208	HOMO->*L* + 1 (89 %), H-1->LUMO (9 %)

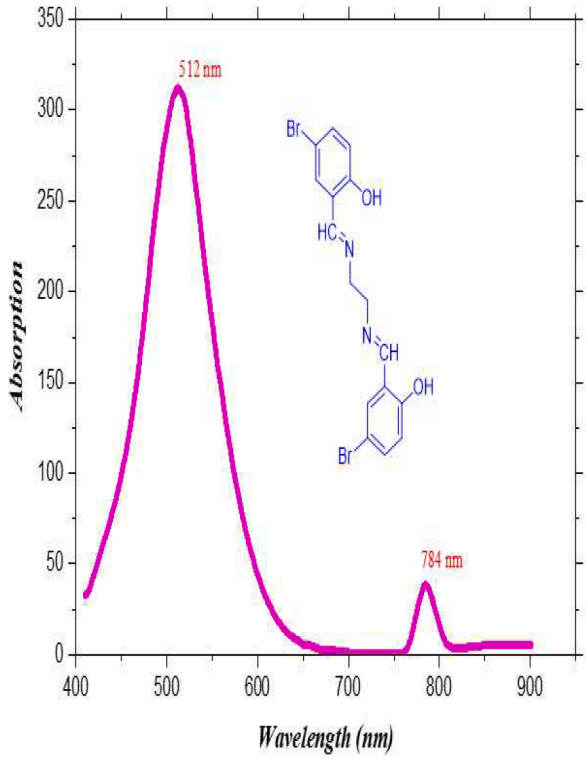

Fig. 8. Fluorescence spectra of 2,2′-((1E,1′E)-(ethane-1,2-diylbis(azaneylylidene)) bis (methaneylylidene)) bis(4-bromophenol).

conformational analysis we choose the highest energy, because highest energy values structure is the most stable [22,23]. Based on the conformational analysis we find the probable energy value and ring energy vale, which is 31.1857 kcal/mol and 24.202 kcal/mol respectively [24]. All of the DFT calculations we used B3LYP/cc-pVDZ basis set, with gas phase [25]. The synthesized compound best optimized structure was presented in Fig. 2, and structural analysis are presented in Table.S1 [26]. In this study we discussed highest bond length bond angle and dihedral angle only, the highest bond angles are C17-Br22 (1.9175 A°), N13-C14-C15 (122.1325 A°) and C4-C3-C5-H24 (179.9979 A°) respectively. The remaining structural parameters are presented in Table.S1.

Solvation study

The LED is important study to find the hydrogen bond (non-covalent) interaction. The water (H_2O) was placed near the -OH functional group. Water molecule is more possible to form a hydrogen bond [27]. The 5BRSET-water complex structure was optimized using ORCA-5 software, with PBE0/D3/def2-TZVP basis sets. After optimization the optimized structure is calculated by local energy decomposition analysis. The calculated solvation study energies are presented in Table 1 [28]. The Schiff base with water molecule hydrogen bond interaction shown in Fig. 3. In Fig. 3 represent the colour blue is non-covalent interaction, red is stirric effect and colour green is Vander Wall interaction [29]. We used ORCA software for LED calculation, which is free software. In the first step, we use the formula $E_{int} = E_{optdimer} - E_{optmonomer}$ to figure out the interaction energy. Lastly, we find out the final interaction energy, using this formula, $DE = DE_{geo\text{-}prep} + DE_{refel\text{-}prep} + E_{refelstat} + E_{refexch} + DEC\text{–}CCSD_{no\text{-}disp} + EC\text{–}CCSD_{disp} + DEC\text{-}(T)_{int}$. The final interaction energy is −9.19 kcal/mol.

Vibrational analysis

The simulated vibrational analysis we used B3LYP/cc-pVDZ basis set level of theory. Infrared spectrum (simulated and experimental) are shown in Fig. 4. The compound 5BRSET has 36 atoms and shows 102 different types of vibrations [30]. According to the C1 point group, it has 35 modes of stretching, 34 modes of bending, and 33 modes of torsion vibrations. The scale factor 0.9651 is used to compare the simulated and experimental spectra [31,32]. The VEDA4 software was used to calculated the PED analysis. In Table 2 presented detailed simulated and experimental FTIR spectral analysis and also PED analysis [33]. In this synthesized compound the -OH stretching frequency is observed at 2852 cm^{-1} in experimental and calculated part -OH stretching frequency is 2853 and 2847 cm^{-1}, with PED contributions are 93 % and 93 % respectively.

The -HC═N- stretching vibration normally present between the range of 1680 and 1640 cm^{-1}, but in this case the -HC═N- str vibration is observed in 1634 cm^{-1} for experimental and related computational part is 1603 and 1601 cm^{-1}, PED is 52 % and 44 % respectively [34]. The experimental -HC- str are presented at 3064, 2923 and 2872 cm^{-1}, and related are 3106, 3105, 3089, 3088, 3078, 3077, 2955, 2953, 2931, 2930, 2887 and 2882 cm^{-1}, with PED involvement of 98 %, 98 %, 97 %, 97 %, 98 %, 98 %, 93 %, 78 %, 96 %, 99 %, 74 % and 99 % respectively. The -HC- in-plane bending vibrations are experimentally observed in the rage of 1305, 1291, 1240, 1217, 1184, 1114, 1079 and 1033 cm^{-1}. The out-plane bending is 978, 913, 895, 825 and 776 cm^{-1} respectively [35]. The titled compound -CBr stretching vibrations is observed in the rage of 628 cm^{-1} in experimental and related computational part is 615, with PED contribution is 14 % respectively.

NMR analysis

The NMR spectroscopy is most important one to confirm the

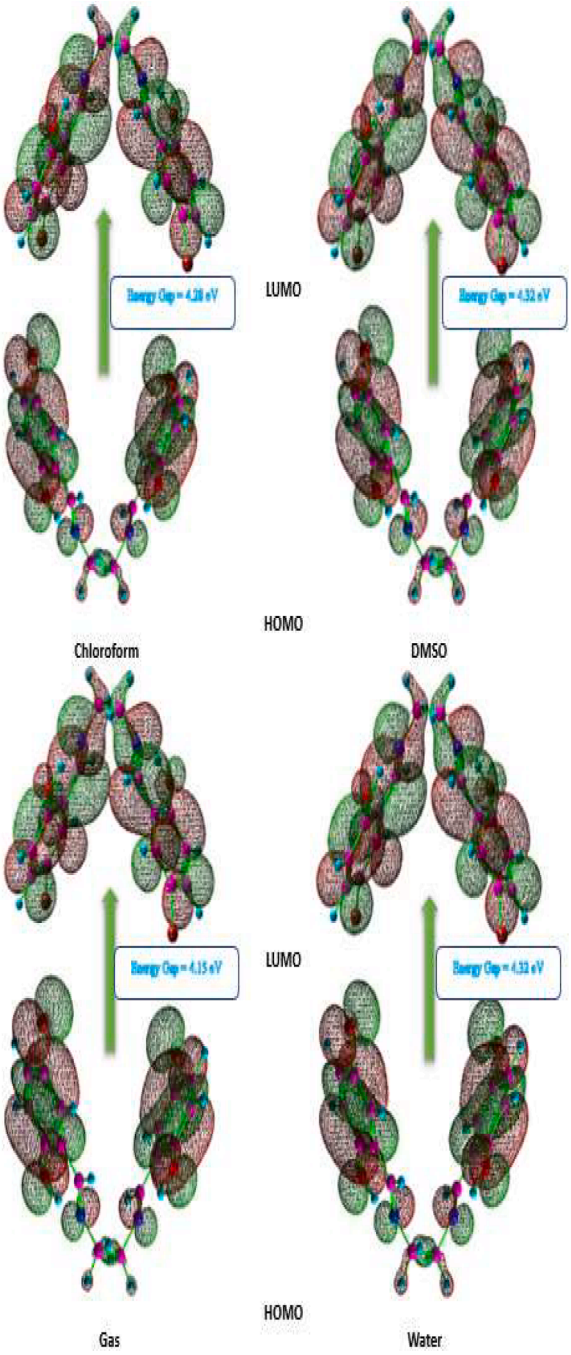

Fig. 9. HOMO-LUMO surface map of 2,2′-((1E,1′E)-(ethane-1,2-diylbis(azaneylylidene)) bis (methaneylylidene)) bis(4-bromophenol).

synthesized compounds structure. Through NMR analysis the range between 0 and 5 ppm the aliphatic proton is presented and 6–12 ppm aromatic proton is presented [36]. The synthesized compound ^{1}HNMR and ^{13}CNMR analysis was done with 400 MHz in chloroform solvent. To figure out the ^{1}HNMR and ^{13}CNMR shifts, DFT calculation was done [37]. The three different peaks that were seen in the ^{1}HNMR spectrum such as singlet, doublet, and multiplet. The ^{1}HNMR were displayed in Fig. 5. In the experimental section, the singlet chemical shift of the azomethine group (-HC═N-) was determined to be 8.58 (s,1H) ppm, while the calculated value was found to be 8.48 (26H, 32H) ppm [38]. The chemical shift of OH was measured to be 13.45 (s,1H)ppm, and the related simulated chemical shift was estimated to be 13.12 (27H, 36H) ppm. The experimental shift of the ethyl group (-H_2C) is 3.93 (s,2H) ppm, and the calculated shifts are 4.01 (28H, 31H) and 4.75 (29H, 30H) respectively.

The chemical shift in ^{13}CNMR for carbon that has an aromatic group is between the 110 and 170 ppm [39]. In Fig. 6 we presented the ^{13}CNME chemical shift. The -HC═N- chemical shift of this compound was measured to be 166.20 ppm and computatational parts to be 155.79 (C7, C14) ppm respectively [39]. The ethyl group was experimentally observed at 58.93 ppm, and related computational part is 54.09 (C11, C12) ppm respectively. The hydroxyl (-OH) group at 160.48 ppm, and related simulated chemical shift is 150.65 (4C, 20C) ppm respectively.

NLO properties

In organic materials may have significant nonlinear optical properties due to the spread out electrons in the n–π* orbitals [40]. The polarizability and hyperpolarizability are used as quantitative ways to connect the structure. The DFT method was used to figure out the NLO properties of the organic compound [41]. It was found that these properties change based on the solvent used [42]. The 5BRSET had a bigger dipole moment value, when compared to urea. The gas phase dipole moment value of the synthesized molecule was 3.435000 D. Also, the dipole moment of chloroform is 4.350400 D, the dipole moment of DMSO is 4.721300 D, and the dipole moment of water is 4.740700 D respectively. Due to the solvent effect the water dipole mement value is higher.

Electronic spectra

By analysing the UV–vis spectrum, the electronic transition features of 5BRSET were found (through experiment and simulated). The titled compound simulated UV spectrum created by Gaussian software using B3LYP/cc-pVDZ basis set [43]. In this study we calculate synthesized compound anti-bonding, bonding and non-bonding characteristics [44]. UV light absorption causes large orbital shifts from HOMO to LUMO in all characteristics [45]. In Fig. 7 we presented the synthesized compound UV–Visible spectrum with experimental, gas phase and different solvent phase. The titled compound simulated absorption wavelength, oscillator strength, energy and bond gap are presented in Table 3. In experimental section predicted absorption wavelength is 391 nm, 329 nm and 320 nm with oscillator strength is 0.0560, 0.3540 and 4.0000, which is recorded from chloroform solvent [46]. The water solvent simulated is 325.920287688 nm, 320.35382316 and 309.973840291 nm, with oscillator strength of 0.1395, 0.0401 and 0.0208 respectively. The gas phase is 337.764831339, 332.617938671, and 322.310907114 nm respectively. Furthermore the chloroform and DMSO solvent absorption peaks are presented at 330.138028597, 324.691205027, 313.667459305 nm and 326.443751026, 320.89276248, 310.245318519 nm respectively. The wavelength is 337.764831339 nm, and energy is 29,606.39792 cm^{-1}, with the band gap is 4.1563 eV were observed in gas phase, the major contribution of this wavelength is HOMO->LUMO (94 %), H-1->L + 1 (4 %) respectively. The main contributions of solvents like chloroform, DMSO, and water are: HOMO-->LUMO (91 %), H-1->L + 1 (7 %), HOMO->LUMO (91 %), H-1->L + 1 (7 %) and HOMO->LUMO (91 %), H-1->L + 1 (6 %) respectively. Table 3 also shows the other major contributions of HOMO and LUMO.

Emission (fluorescence) spectrum

Electrons shift from ground to an excited state in light that is either visible or ultraviolet. Because the atom is unstable, it will emit ultraviolet or visible light, returning it to its singlet ground state [47]. Fluorophores emit light as they transition from their excited to their ground states [48]. The 5BRSET fluorescence spectrum (Fig. 8) displays two peaks at 512 nm and 784 nm. These spots illustrate the molecule emitting light, and absorption light was emitted at 329 nm [49]. Fluorescence takes place when a molecule absorbs light and emits it with a

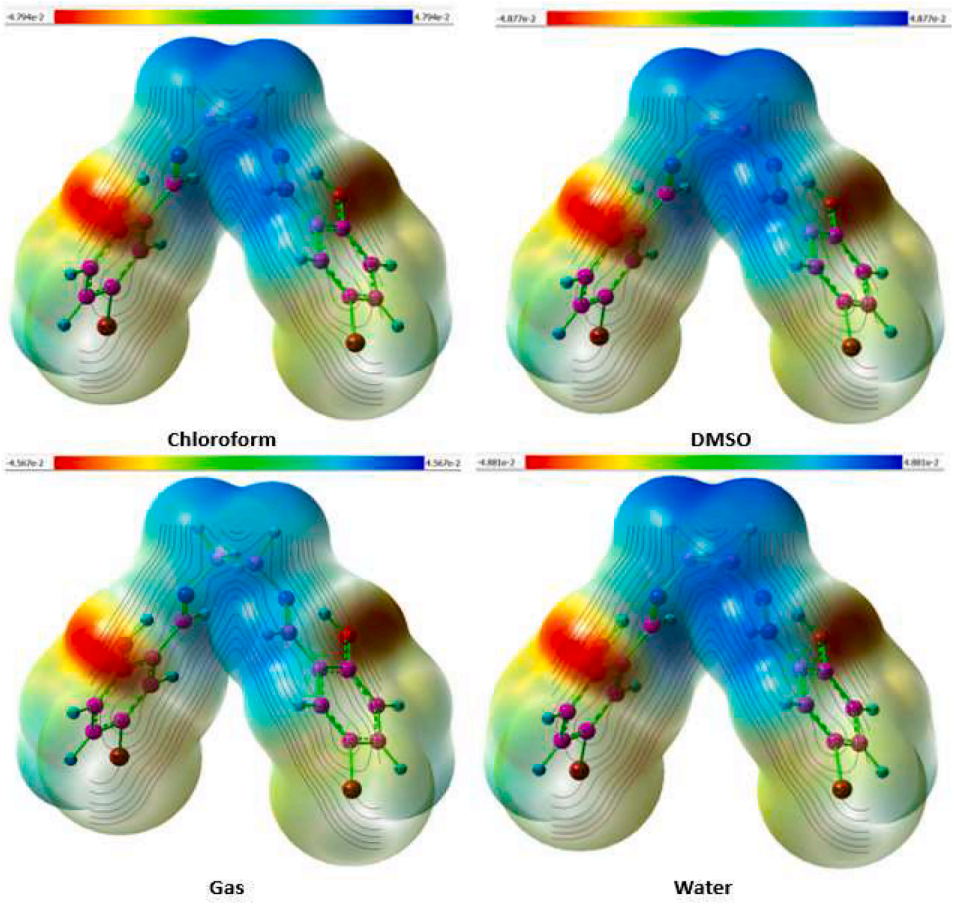

Fig. 10. MEP surface map of 2,2′-((1E,1′E)-(ethane-1,2-diylbis(azaneylylidene)) bis (methaneylylidene)) bis(4-bromophenol).

longer wavelength. The structure of this molecule can absorb 329 nm light and emit 512 nm light. Two fluorescence peaks indicate that the substance is stimulated in two ways. Both states degrade differently and emit different light [50]. The molecule electrons may be in different places or shapes, changing its energy levels and how it flows between them. The fluorescence radiation spectrum reveals molecular and electrical characteristics.

FMO study

FMO analysis are mainly used to identify the intramolecular charge transfer. The Gauss view-6 programme was used to figure out the global variables, which are shown in Fig. 9 and listed in Table S2 for analysis in different solvents (chloroform, DMSO and water) [51]. The difference in energy between the HOMO and LUMO states proves that the molecule has both soft and hard qualities. In general, the smaller a molecule energy gap, the softer and more polarizable it is, the more chemically reactive it is, and the less stable it is in motion. When molecules were put in solvents, it was found that the energy gaps controlled in one direction [52]. The named chemical has an energy gap of 4.16 eV in gas phase, 4.28 in chloroform, 4.33 in DMSO, and 4.33 in water. Generally, higher the energy gap value, compounds exhibit low chemical reactivity and high kinetic stability and lower the energy gap values compounds exhibit higher chemical reactivity and lower kinetic stability. In this titled compound the energy gap value is higher, it means the titled compound lower chemical reactivity and higher kinetic stability [53]. When compared to gas phase and other solvent DMSO has the highest energy gap value. The gas phase electronegativity is calculated to be 3.77 eV and the electron affinity is calculated to be 1.70 eV [54]. These numbers are very low compared to the gas phase ionisation potential, which is 5.85 eV [55]. The synthesized compound gas phase electrophilicity index is 3.85 eV, this values identify the toxic and reactive sites of the compound. This shows that the chemical isn't harmful. Based on the determined global descriptors, the 5BRSET molecule has great biological properties in terms of pharmacology.

Molecular electrostatic potential

In this study we identify the electrophilic and nucleophilic attacking sites, molecular structure surrounding hydrogen bonding, and electron density [56]. The Molecular Electrostatic Potential (MEP) refers to the determination of the energy of interaction between the charge distribution of a molecule and a unit positive charge [57]. Using DFT and the B3LYP/cc-pVDZ method, the 5BRSET molecular electrostatic potential was calculated [58]. Fig. 10 MEP shown in which place electrophilic and nucleophilic interactions are presented [59]. In the gas phase, the molecular electrostatic potential range from –4.567 e^{-2} to 4.567 e^{-2}. Also, the electrostatic potential ranges of −4.794 e^{-2} to 4.794 e^{-2} for chloroform, −4.877 e^{-2} to 4.877 e^{-2} for DMSO, and −4.881 e^{-2} to 4.881 e^{-2} for water. When compare to other solvents the water electrostatic potential range is higher. The colour blue show in -OH group, it represented at the electrophilic attack. The yellow colour shown from the carbon in the benzyl ring.

Mulliken population study

Charge distribution analysis influences charge communications, structure electrostatic potential, and chemical reactions. The NPA and MPA provide information about the electron distribution within a molecule [60]. Atoms gain the electrons to become negatively charged.

Table 4
Natural bond orbital analysis of 2,2′-((1E,1′E)-(ethane-1,2-diylbis(azaneylylidene)) bis (methaneylylidene)) bis(4-bromophenol).

Donar	Type	ED/e	Acceptor	Type	ED/e	E(2)[a]	E(j-i)[b]	F(i,j)[c]
C 1 - C 2	σ	1.97924	C 1 - C 6	σ*	0.02727	3.84	1.29	0.063
			C 2 - C 3	σ*	0.02203	3.24	1.3	0.058
			C 2 - H 23	σ*	0.01471	1.78	1.18	0.041
			C 3 - C 7	σ*	0.02711	3.24	1.23	0.056
			C 6 - H 25	σ*	0.01349	2.39	1.19	0.048
C 1 - C 2	π	1.72107	C 5 - C 6	π*	0.30869	21.27	0.31	0.072
C 1 - C 6	σ	1.97928	C 1 - C 2	σ*	0.02435	3.98	1.31	0.064
			C 2 - H 23	σ*	0.01471	2.76	1.17	0.051
			C 5 - C 6	σ*	0.01499	2.69	1.31	0.053
			C 5 - H 24	σ*	0.01287	2.45	1.18	0.048
			C 6 - H 25	σ*	0.01349	1.42	1.18	0.037
C 1 -Br 9	σ	1.98402	C 2 - C 3	σ*	0.02203	3.61	1.22	0.059
			C 5 - C 6	σ*	0.01499	3.21	1.24	0.056
C 2 - C 3	σ	1.96257	C 1 - C 2	σ*	0.02435	3.66	1.28	0.061
			C 1 -Br 9	σ*	0.03433	5.35	0.78	0.058
			C 2 - H 23	σ*	0.01471	1.07	1.14	0.031
			C 3 - C 4	σ*	0.04	3.71	1.24	0.061
			C 3 - C 7	σ*	0.02711	2.74	1.19	0.051
			C 4 - O 8	σ*	0.02019	3.61	1.08	0.056
			C 7 - N 10	σ*	0.00978	1.82	1.29	0.044
C 2 - H 23	σ	1.97675	C 1 - C 2	σ*	0.02435	1.01	1.11	0.03
			C 1 - C 6	σ*	0.02727	4.53	1.08	0.063
			C 2 - C 3	σ*	0.02203	0.83	1.09	0.027
			C 3 - C 4	σ*	0.04	4.74	1.07	0.064
C 3 - C 4	σ	1.97151	C 2 - C 3	σ*	0.02203	3.68	1.26	0.061
			C 2 - H 23	σ*	0.01471	2.34	1.14	0.046
			C 3 - C 7	σ*	0.02711	2.8	1.2	0.052
			C 4 - C 5	σ*	0.02541	3.42	1.27	0.059
			C 5 - H 24	σ*	0.01287	2.28	1.16	0.046
			C 7 - H 26	σ*	0.03525	1.76	1.12	0.04
C 3 - C 7	σ	1.97085	C 1 - C 2	σ*	0.02435	2.66	1.27	0.052
			C 2 - C 3	σ*	0.02203	2.97	1.25	0.054
			C 3 - C 4	σ*	0.04	2.71	1.23	0.052
			C 4 - C 5	σ*	0.02541	2.65	1.25	0.051
			C 7 - N 10	σ*	0.00978	1.86	1.28	0.044
			N 10 - C 11	σ*	0.02374	4.57	1.04	0.062
C 4 - C 5	σ	1.97515	C 3 - C 4	σ*	0.04	3.51	1.25	0.059
			C 3 - C 7	σ*	0.02711	3.61	1.2	0.059
			C 4 - O 8	σ*	0.02019	0.53	1.08	0.021
			C 5 - C 6	σ*	0.01499	2.53	1.29	0.051
			C 5 - H 24	σ*	0.01287	1.12	1.16	0.032
			C 6 - H 25	σ*	0.01349	2.56	1.16	0.049
			O 8 - H 27	σ*	0.08298	2.41	1.1	0.047
C 4 - O 8	σ	1.99389	C 2 - C 3	σ*	0.02203	1.85	1.49	0.047
			C 3 - C 4	σ*	0.04	0.9	1.48	0.033
			C 4 - C 5	σ*	0.02541	0.94	1.5	0.034
			C 5 - C 6	σ*	0.01499	1.67	1.52	0.045
C 5 - C 6	σ	1.96895	C 1 - C 6	σ*	0.02727	3.43	1.26	0.059
			C 1 -Br 9	σ*	0.03433	5.09	0.79	0.057
			C 4 - C 5	σ*	0.02541	2.43	1.27	0.05
			C 4 - O 8	σ*	0.02019	3.51	1.09	0.055
			C 5 - H 24	σ*	0.01287	1.37	1.17	0.036
			C 6 - H 25	σ*	0.01349	1.19	1.16	0.033
C 5 - C 6	π	1.70047	C 1 - C 2	π*	0.37242	16.5	0.28	0.061
C 5 - H 24	σ	1.97595	C 1 - C 6	σ*	0.02727	4.52	1.07	0.062
			C 3 - C 4	σ*	0.04	4.71	1.06	0.063
			C 4 - C 5	σ*	0.02541	0.57	1.08	0.022
			C 4 - O 8	σ*	0.02019	0.95	0.89	0.026
			C 5 - C 6	σ*	0.01499	0.83	1.11	0.027
C 6 - H 25	σ	1.97775	C 1 - C 2	σ*	0.02435	4.48	1.11	0.063
			C 1 - C 6	σ*	0.02727	0.72	1.08	0.025
			C 4 - C 5	σ*	0.02541	4.24	1.09	0.061
			C 5 - C 6	σ*	0.01499	0.82	1.11	0.027
C 7 - N 10	σ	1.98812	C 2 - C 3	σ*	0.02203	2.19	1.46	0.051
			C 3 - C 7	σ*	0.02711	1.75	1.39	0.044
			C 7 - H 26	σ*	0.03525	0.63	1.31	0.026
			O 8 - H 27	σ*	0.08298	1.38	1.29	0.038
			N 10 - C 11	σ*	0.02374	1.44	1.26	0.038
			C 11 - C 12	σ*	0.02397	0.57	1.26	0.024
C 7 - N 10	π	1.94236	C 11 - C 12	σ*	0.02397	3.51	0.71	0.045
			C 11 - H 29	σ*	0.01540)	2.85	0.78	0.043
C 7 - H 26	σ	1.98637	C 3 - C 4	σ*	0.04	4.34	1.09	0.062
O 8 - H 27	σ	1.98379	C 4 - C 5	σ*	0.02541	6.01	1.29	0.079
			N 10 - C 11	σ*	0.02374	0.85	1.09	0.027

(*continued on next page*)

Table 4 (*continued*)

Donar	Type	ED/e	Acceptor	Type	ED/e	E(2)[a]	E(j-i)[b]	F(i,j)[c]
N 10 - C 11	σ	1.98246	C 3 - C 7	σ*	0.02711	4.22	1.23	0.065
			C 7 - N 10	σ*	0.00978	1.48	1.33	0.04
			C 12 - H 30	σ*	0.0154	1.34	1.18	0.035
C 11 - C 12	σ	1.96512	C 7 - N 10	σ*	0.00978	1.52	1.22	0.039
			C 7 - N 10	π*	0.15883	2	0.62	0.033
			N 13 - C 14	σ*	0.00978	1.52	1.22	0.039
			N 13 - C 14	π*	0.15883	2	0.62	0.033
C 11 - H 28	σ	1.98298	C 3 - C 7	σ*	0.02711	0.55	1	0.021
			C 12 - N 13	σ*	0.02373	0.51	0.87	0.019
			C 12 - H 31	σ*	0.02584	3.11	0.94	0.048
C 11 - H 29	σ	1.96567	C 7 - N 10	σ*	0.00978	2.18	1.1	0.044
			C 7 - N 10	π*	0.15883	2.84	0.51	0.035
			C 12 - N 13	σ*	0.02373	4.23	0.87	0.054
C 12 - N 13	σ	1.98246	C 11 - H 29	σ*	0.0154	1.34	1.18	0.035
			N 13 - C 14	σ*	0.00978	1.48	1.33	0.04
			C 14 - C 15	σ*	0.02711	4.22	1.23	0.065
C 12 - H 30	σ	1.96567	N 10 - C 11	σ*	0.02374	4.23	0.87	0.054
			N 13 - C 14	σ*	0.00978	2.18	1.1	0.044
			N 13 - C 14	π*	0.15883	2.84	0.51	0.035
C 12 - H 31	σ	1.98298	N 10 - C 11	σ*	0.02374	0.51	0.87	0.019
			C 11 - H 28	σ*	0.02584	3.11	0.94	0.048
			C 14 - C 15	σ*	0.02711	0.55	1	0.021
N 13 - C 14	σ	1.98812	C 11 - C 12	σ*	0.02397	0.57	1.26	0.024
			C 12 - N 13	σ*	0.02373	1.44	1.26	0.038
			C 14 - C 15	σ*	0.02711	1.75	1.39	0.044
			C 14 - H 32	σ*	0.03525	0.63	1.31	0.026
			C 15 - C 16	σ*	0.02203	2.19	1.46	0.051
			O 21 - H 36	σ*	0.08298	1.38	1.29	0.038
N 13 - C 14	π	1.94236	C 11 - C 12	σ*	0.02397	3.51	0.71	0.045
			C 12 - H 30	σ*	0.0154	2.85	0.78	0.043
C 14 - C 15	σ	1.97085	C 12 - N 13	σ*	0.02373	4.57	1.04	0.062
			N 13 - C 14	σ*	0.00978	1.86	1.28	0.044
			C 15 - C 16	σ*	0.02203	2.97	1.25	0.054
			C 15 - C 20	σ*	0.04	2.71	1.23	0.052
			C 16 - C 17	σ*	0.02435	2.66	1.27	0.052
			C 19 - C 20	σ*	0.02541	2.65	1.25	0.051
C 14 - H 32	σ	1.98637	C 15 - C 20	σ*	0.04	4.34	1.09	0.062
C 15 - C 16	σ	1.96257	N 13 - C 14	σ*	0.00978	1.82	1.29	0.044
			C 14 - C 15	σ*	0.02711	2.74	1.19	0.051
			C 15 - C 20	σ*	0.04	3.71	1.24	0.061
			C 16 - C 17	σ*	0.02435	3.66	1.28	0.061
			C 16 - H 33	σ*	0.01471	1.07	1.14	0.031
			C 17 -Br 22	σ*	0.03433	5.35	0.78	0.058
			C 20 - O 21	σ*	0.02019	3.61	1.08	0.056
C 15 - C 20	σ	1.97151	C 14 - C 15	σ*	0.02711	2.8	1.2	0.052
			C 14 - H 32	σ*	0.03525	1.76	1.12	0.04
			C 15 - C 16	σ*	0.02203	3.68	1.26	0.061
			C 16 - H 33	σ*	0.01471	2.34	1.14	0.046
			C 19 - C 20	σ*	0.02541	3.42	1.27	0.059
			C 19 - H 35	σ*	0.01287	2.28	1.16	0.046
C 16 - C 17	σ	1.97924	C 14 - C 15	σ*	0.02711	3.24	1.23	0.056
			C 15 - C 16	σ*	0.02203	3.24	1.3	0.058
			C 16 - H 33	σ*	0.01471	1.78	1.18	0.041
			C 17 - C 18	σ*	0.02727	3.84	1.29	0.063
			C 18 - H 34	σ*	0.01349	2.39	1.19	0.048
C 16 - C 17	π	1.72107	C 18 - C 19	π*	0.30869	21.27	0.31	0.072
C 16 - H 33	σ	1.97675	C 15 - C 16	σ*	0.02203	0.83	1.09	0.027
			C 15 - C 20	σ*	0.04	4.74	1.07	0.064
			C 16 - C 17	σ*	0.02435	1.01	1.11	0.03
			C 17 - C 18	σ*	0.02727	4.53	1.08	0.063
C 17 - C 18	σ	1.97928	C 16 - C 17	σ*	0.02435	3.98	1.31	0.064
			C 16 - H 33	σ*	0.01471	2.76	1.17	0.051
			C 18 - C 19	σ*	0.01499	2.69	1.31	0.053
			C 18 - H 34	σ*	0.01349	1.42	1.18	0.037
			C 19 - H 35	σ*	0.01287	2.45	1.18	0.048
C 17 -Br 22	σ	1.98402	C 15 - C 16	σ*	0.02203	3.61	1.22	0.059
			C 18 - C 19	σ*	0.01499	3.21	1.24	0.056
C 18 - C 19	σ	1.96895	C 17 - C 18	σ*	0.02727	3.43	1.26	0.059
			C 17 -Br 22	σ*	0.03433	5.09	0.79	0.057
			C 18 - H 34	σ*	0.01349	1.19	1.16	0.033
			C 19 - C 20	σ*	0.02541	2.43	1.27	0.05
			C 19 - H 35	σ*	0.01287	1.37	1.17	0.036
			C 20 - O 21	σ*	0.02019	3.51	1.09	0.055
C 18 - C 19	π	1.70047	C 16 - C 17	π*	0.37242	16.5	0.28	0.061
C 18 - H 34	σ	1.97775	C 16 - C 17	σ*	0.02435	4.48	1.11	0.063
			C 17 - C 18	σ*	0.02727	0.72	1.08	0.025

(*continued on next page*)

Table 4 (*continued*)

Donar	Type	ED/e	Acceptor	Type	ED/e	E(2)[a]	E(j-i)[b]	F(i,j)[c]
			C 18 - C 19	σ*	0.01499	0.82	1.11	0.027
			C 19 - C 20	σ*	0.02541	4.24	1.09	0.061
C 19 - C 20	σ	1.97515	C 14 - C 15	σ*	0.02711	3.61	1.2	0.059
			C 15 - C 20	σ*	0.04	3.51	1.25	0.059
			C 18 - C 19	σ*	0.01499	2.53	1.29	0.051
			C 18 - H 34	σ*	0.01349	2.56	1.16	0.049
			C 19 - H 35	σ*	0.01287	1.12	1.16	0.032
			C 20 - O 21	σ*	0.02019	0.53	1.08	0.021
			O 21 - H 36	σ*	0.08298	2.41	1.1	0.047
C 19 - H 35	σ	1.97595	C 15 - C 20	σ*	0.04	4.71	1.06	0.063
			C 17 - C 18	σ*	0.02727	4.52	1.07	0.062
			C 18 - C 19	σ*	0.01499	0.83	1.11	0.027
			C 19 - C 20	σ*	0.02541	0.57	1.08	0.022
			C 20 - O 21	σ*	0.02019	0.95	0.89	0.026
C 20 - O 21	σ	1.99389	C 15 - C 16	σ*	0.02203	1.85	1.49	0.047
			C 15 - C 20	σ*	0.04	0.9	1.48	0.033
			C 18 - C 19	σ*	0.01499	1.67	1.52	0.045
			C 19 - C 20	σ*	0.02541	0.94	1.5	0.034
O 21 - H 36	σ	1.98379	C 12 - N 13	σ*	0.02373	0.85	1.09	0.027
			C 19 - C 20	σ*	0.02541	6.01	1.29	0.079
LP (1)	C 3	1.09906	C 1 - C 2	π*	0.37242	84	0.14	0.111
LP (1)	O 8	1.96999	C 3 - C 4	σ*	0.04	7.88	1.11	0.084
LP (1)	Br 9	1.99356	C 1 - C 2	σ*	0.02435	1.56	1.57	0.044
LP (2)	Br 9	1.97584	C 1 - C 2	σ*	0.02435	3.01	0.88	0.046
LP (3)	Br 9	1.94784	C 1 - C 2	π*	0.37242	9.01	0.31	0.051
LP (1)	N 10	1.85459	C 3 - C 7	σ*	0.02711	2.17	0.87	0.04
LP (1)	N 13	1.85459	C 12 - H 30	σ*	0.0154	0.63	0.81	0.021
LP (1)	C 15	1.09906	N 13 - C 14	π*	0.15883	63.45	0.13	0.101
LP (1)	O 21	1.96999	C 15 - C 20	σ*	0.04	7.88	1.11	0.084
LP (1)	Br 22	1.99356	C 16 - C 17	σ*	0.02435	1.56	1.57	0.044
LP (2)	Br 22	1.97584	C 16 - C 17	σ*	0.02435	3.01	0.88	0.046
LP (3)	Br 22	1.94784	C 16 - C 17	π*	0.37242	9.01	0.31	0.051

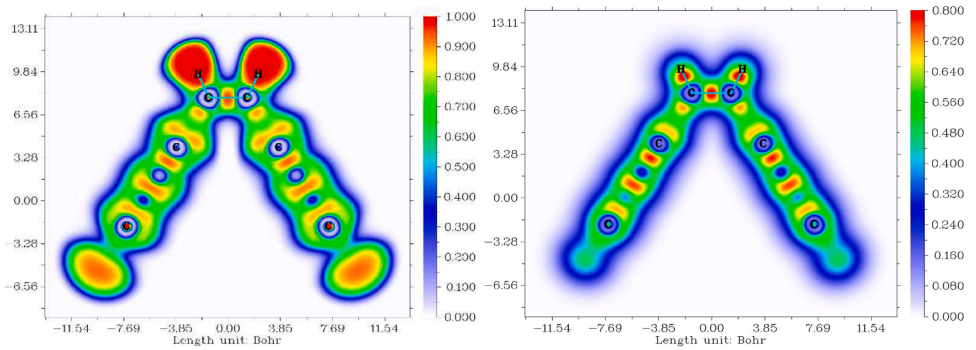

Fig. 11. ELF and LOL surface map of 2,2′-((1E,1′E)-(ethane-1,2-diylbis(azaneylylidene)) bis (methaneylylidene)) bis(4-bromophenol).

Positively charged atoms lose the electrons. This study shows that the molecule can operate as an electrophile and a nucleophile using the MPA and NPA [61]. Table S3 shows the Mulliken atomic charges, whereas Table S4 looks at the natural population analysis [62]. The 27H (0.144671) atom is most positive charge and 10 N (−0.28494) atom is most negative charge in MPA analysis. Every atom of carbon and hydrogen has both positive and negative charges [63]. The electronegative atom O, Br and N have the negative charge only for MPA analysis. The atom with the most positive charge in NPA is 27H, which has a charge of 0.50884. The atom with the most negative charge is O21, which has a charge of −0.70647 respectively. The atom N and O is electronegative, which means it has negative charge. The carbon atom have both positive and negative charge. Hydrogen and bromine has positive charge only in NPA analysis.

NBO analysis

Natural bond orbital analysis can be used to study the inter and intra molecular bond properties. The computational study of NBO analysis were done by B3LYP/ccp-VDZ basis set using Gaussian software [64,65]. Both Lewis and non-Lewis NBO orbitals delocalize electron density [66]. Non-Lewis NBOs eliminate the bonds, while Lewis NBO make bonds. Solid electron delocalization is shown through Lewis structure donor--acceptor interactions [67]. In this investigation, we found that molecules interact and electrons travel and mix within the molecules. Table 4 shows how the NBO study of the titled molecule. In a conjugated system, single and double bond electron densities allow for measuring molecular distance. The NBO result shows that 205.17203 205.17203 (97.701 % of 210) in the molecule are in the Lewis structure and 4.82797 (2.299 % of 210) are in the non-Lewis structure [68].

The NBO study (Table 4) found that the s(C1–C2) bond appears in

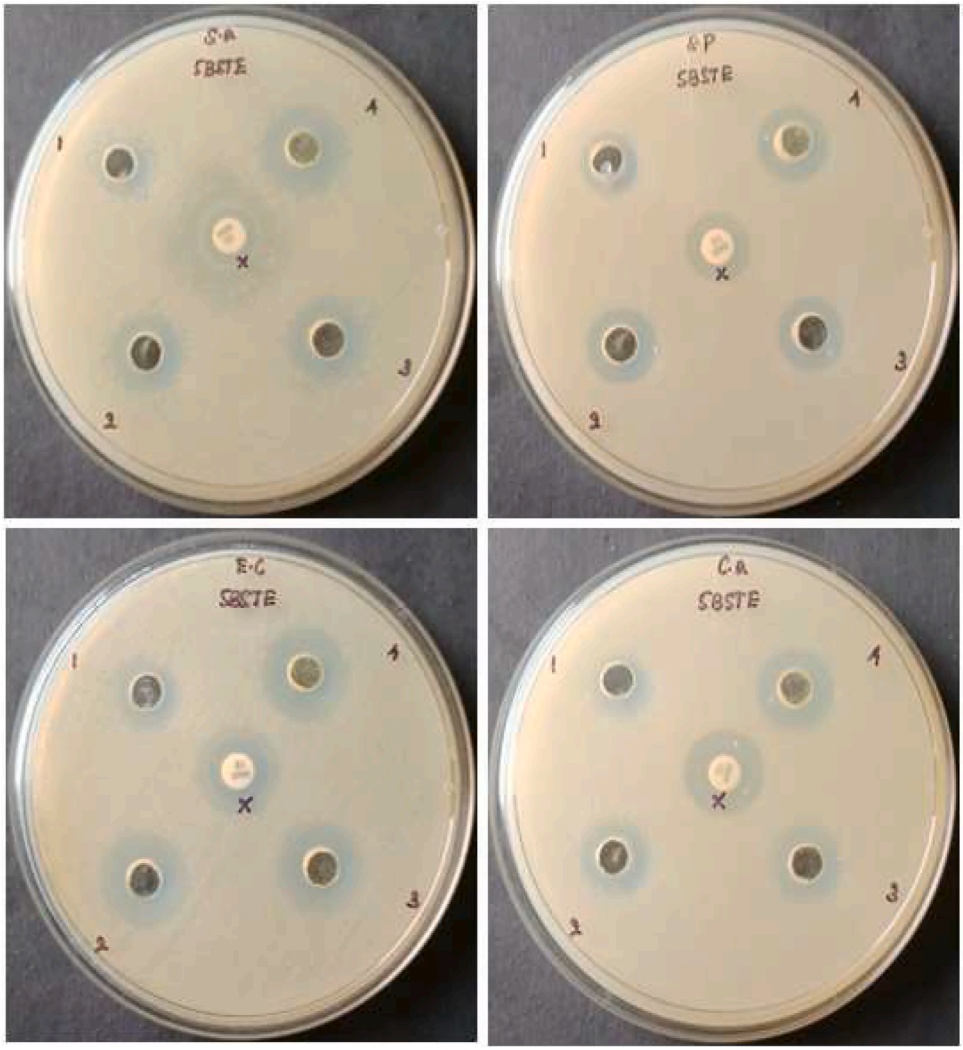

Fig. 12. Antimicrobial activity of 2,2′-((1E,1′E)-(ethane-1,2-diylbis(azaneylylidene)) bis (methaneylylidene)) bis(4-bromophenol).

Table 5
Antibacterial and antifungal activity inhibition zone of 2,2′-((1E,1′E)-(ethane-1,2-diylbis(azaneylylidene)) bis (methaneylylidene)) bis(4-bromophenol).

Sample	Bac name	1 mg/ml	1.5 mg/ml	2 mg/ml	2.5 mg/ml	Amoxicillin
5BRSTE	***S. aureus***	11	13.5	16	17.5	21.5
5BRSTE	***S. pneumoniae***	11	13.5	12	13.5	14.5
5BRSTE	***E.coli***	12	14	16.5	17.5	16.5
5BRSTE	***C. albicans***	11	12.5	13	14.5	15.5

carbon $sp^{1.53}$ hybrid orbital (60.40 % *p*-character) interacts with a carbon $sp^{1.78}$ hybrid (63.97 % *p*-character) [69]. The s(C1 - Br9) established in carbon $sp^{3.64}$ hybrid orbital (76.09 % *p*-character) contacted with bromine $sp^{5.95}$ (85.31 % p-character). The s(C2–H23) bond developed when carbon $sp^{2.51}$ hybrid orbital (71.50 % *p*-character) reacted with hydrogen $sp^{0.00}$ hybrid orbital (0.07 % *p*-character). The s(C4–O8) bond was generated in the $sp^{2.90}$ hybrid orbital of carbon (74.18 % *p*-character) connected with the $sp^{1.85}$ hybrid orbital (64.8 %). NBO analysis found that the s(C7–N10) bond appears in a carbon $sp^{2.05}$ hybrid orbital (67.18 % *p*-character) contacts with a nitrogen $sp^{1.47}$ hybrid orbital (59.42 % *p*-character) respectively.

The stabilisation energy 63.45 kcal/mol is the highest, which is observed at LP(1) C15 to anti-bonding (N13-C14) with occupancy is 1.09906. furthermore the highest stabilization energies are observed at bonding (C16-C17), (C5-C6) and (C1-C2) to anti-bonding π*(C18-C19), π*(C1-C2) and π*(C5-C6), with occupancy are 1.72107, 1.70047 and 1.72107 and stabilization energies are 21.27, 16.50 and 21.27 kcal/mol respectively.

Topology analysis

The topological analysis explains the synthesized compound localized and delocalized orbital locations. The ELF and LOL are the measured lengths between molecule electron pairs that match the covalent bonds [70]. Extreme localised and delocalized orbital overlap (LOL and ELF) and calculated from orbital slopes [71]. The ELF and LOL colour filled map were generated in Multiwfn software, and presented in Fig. 11. The colours go from blue to crimson. The ELF exhibits a range covering from 0.000 to 1.000, while the range for the LOL goes from 0.000 to 0.800 [66]. The coloured bands visually represent the bonding orbitals. When the value of the colour range is less than 0.5, it is referred to as delocalized in terms of the electronic area. Conversely, when the value exceeds 0.5, it is referred to be localized. The majority of the electrons involved in bonding and non-bonding interactions have a red coloration. The red region corresponds to hydrogen atoms, whereas the blue region corresponds to carbon atoms. The colour pale blue is indicative of the charge and quantity of electrons present in the inner

Table 6
Protein-ligand interaction binding energy of 2,2′-((1E,1′E)-(ethane-1,2-diylbis (azaneylylidene)) bis (methaneylylidene)) bis(4-bromophenol) 5BRSET with 4LEB, 4WJY, 8BXA, 2WMF proteins.

Protein	Rank	Run	Binding energy	Cluster RMSD	Reference RMSD
	1	10	−4.69	0	12.6
	2	7	−4.19	0	25.39
	2	2	−3.87	1.54	25.41
	3	5	−3.76	0	14.22
4LEB	4	6	−3.75	0	26.36
	5	1	−3.46	0	21.48
	6	9	−3.18	0	31.58
	7	4	−2.83	0	26.36
	8	3	−2.58	0	32.97
	9	8	−2.34	0	21.42
	1	6	−4.85	0	57.95
	2	3	−3.38	0	75.15
	3	8	−3.37	0	72.35
	4	9	−3.19	0	46.09
4WJY	5	4	−3.03	0	26.42
	6	1	−2.87	0	83.07
	7	5	−2.54	0	22.22
	8	10	−2.47	0	30.9
	9	2	−1.97	0	74.26
	10	7	−1.78	0	55.92
	1	1	−5.36	0	14.39
	2	2	−5.13	0	10.52
	3	8	−4.31	0	16.83
	4	3	−4.22	0	19.56
8BXA	5	4	−3.82	0	9.68
	6	6	−3.55	0	15.25
	7	5	−2.71	0	17.46
	8	7	−2.42	0	31.24
	9	9	−2.41	0	30.9
	10	10	−1.9	0	34.41
	1	10	−5.13	0	63.05
	2	1	−3.59	0	48.1
	3	6	−3.23	0	48.21
	4	5	−3.17	0	48.75
2WMF	5	7	−2.94	0	62.7
	6	8	−2.88	0	49.46
	7	3	−2.78	0	43.83
	8	4	−2.37	0	70.5
	9	2	−2.16	0	58.43
	10	9	−1.9	0	76.84

shell.

NCI (non-covalent interaction) study

The NCI study is very helpful way to figure out the covalent, intramolecular, and intermolecular hydrogen bonds. In Fig. 12 we represented the titled compound NCI analysis colour filled map [72]. The titled molecule non-covalent interaction were identified and explained [73]. The Fig. 3 we observed three different colours. In colour blue represented the non-covalent (hydrogen bond) interaction, colour red mention the steric effect. Furthermore, the colour green identify the Vander Wall interaction [74]. The NCI plot could interact with 5BRSET through HB interactions between ions and dipoles, interactions between dipoles, interactions between hydrophobic groups, pi-stacking, and van der Waals forces.

Antibacterial action

In this study, Mueller Hinton agar plates were employed to assess the antibacterial activity. In this study, the bacterial strains selected for analysis are *Staphylococcus aureus, Streptococcus pneumoniae*, and *E. coli*. At a concentration of 2.5 mg/ml, the 5BRSET compound was better to control the *E. coli*. Compare the other organisms the *E. coli* is the better antimicrobial activity [75]. Amoxicillin was employed as the reference (standard), and upon comparison, it was found that the synthesized compound exhibited a superior zone of inhibition against *E. coli* when compared to the standard. The standard zone of inhibition is typically observed at a concentration of 16.5 mg/ml. However, the zone of inhibition for our synthesized molecule was found to be 17.5 mg/ml [76]. The antimicrobial activity test were done by four different concentrations like 1, 1.5, 2, and 2.5 mg/ml. The antimicrobial activity of *E. coli* is 12, 14, 16.5 and 17.5 mg/ml, for the concentration of 1, 1.5, 2, and 2.5 mg/ml respectively. The results did not support against *S. aureus* and *S. pneumoniae,* when compared to standard and *E. coli* [77]. *E. coli* (gram negative) microorganism are more activity against our synthesized compound. On the other hand, the 5BRSET not much to better activity against *S. aureus, S. pneumoniae*. The antibacterial activity is shown in Fig. 12 and Table 5.

Antifungal action

The *Candida albicans*, is in antifungal microorganism, has also been linked to several illnesses. But in this study, we used microorganisms from the *Candida albicans* [78]. Fig. 12 shows that different concentrations of synthesized compound and Tble.5 listed the zone of inhibition. Here, *C. albicans* was used to test the antifungal activity against 5BRSET compound [79]. As an antifungal results the synthesized compound 5BRSET is a moderate antifungal activity against *Candida albicans*. We can used four different concentrations such as 1 mg/ml, 1.5 mg/ml, 2 mg/ml, and 2.5 mg/ml, and zone of inhibition was measured at 11, 12.5,

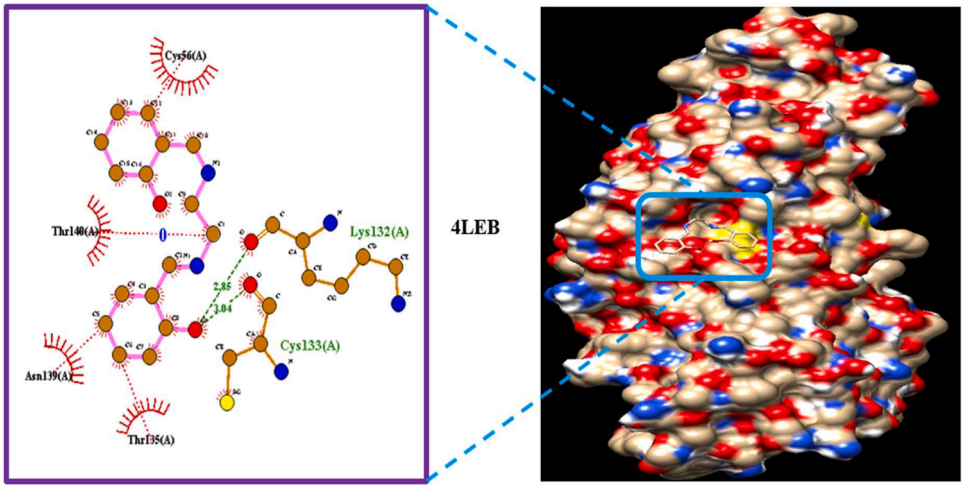

Fig. 13. Protein-ligand interaction sites of 5BRSET with 4LEB protein.

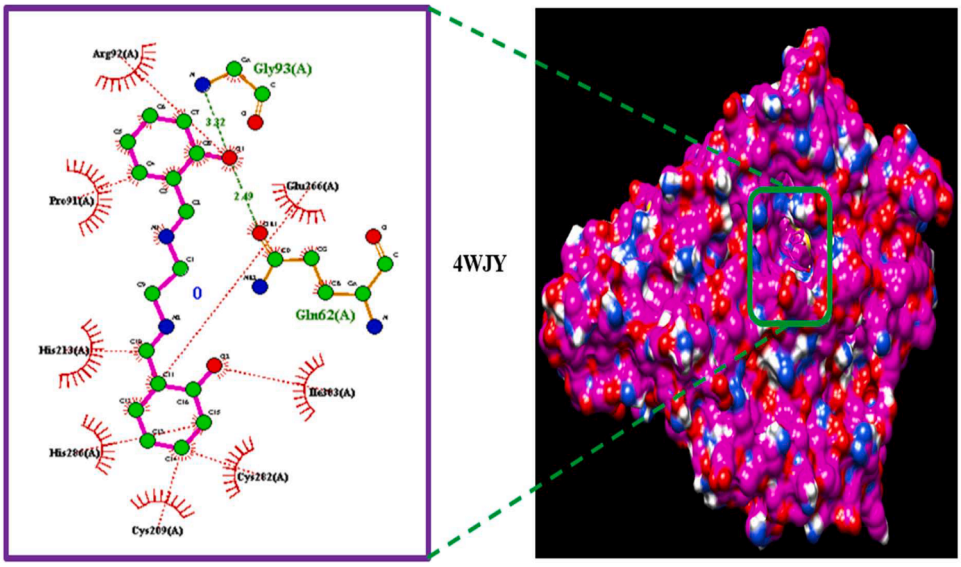

Fig. 13(a). Protein-ligand interaction sites of 5BRSET with 4WJY protein.

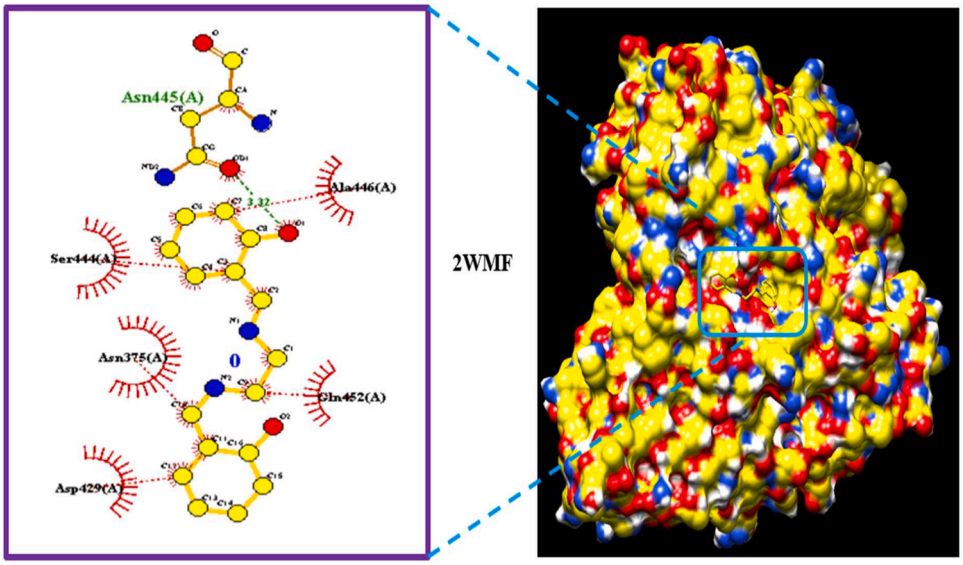

Fig. 13(b). Protein-ligand interaction sites of 5BRSET with 2WMF protein.

13 and 14.5 mg/ml respectively. But the standard zone of inhibition is 15.5 mg/ml, compared to standard our synthesized compound moderate antifungal activity.

Molecular docking study

The physicochemical and drug-like properties of the compound 5BRSET are being studied, which will give us useful knowledge. Lipinski's rule of five was the basis for the identify the chemical compounds physical properties [80]. The Table S5 present the physicochemical properties of the titled compound [81]. Using Swiss ADME online tool the synthesized compound physicochemical properties are calculated [82]. The experimental antimicrobial and antifungal study, who observed our synthesized compound moderate activity. In theoretical study (docking study) also confirmed our synthesized compound lower binding affinity score. In this study we choose four different proteins such as 4LEB (*candida albicans*), 4WJY (*E.coli*), 8BXA (*S.aureaus*), and 2WMF (*S.pheumoniae*). In the experimental antimicrobial section, we studied four different microorganisms, so we can choose four different proteins [83]. Autodock software was used to run the MD simulation. The 4LEB, 4WJY, 8BXA, 2WMF proteins crystal structure was found with the help of the RCSB-PDB online data base. After downloading protein we removed the heatatom and water molecule using discovery studio [84]. The highest binding energy is observed at −4.69, −4.85, −5.36 and −5.13 kcal/mol for 4LEB, 4WJY, 8BXA, and 2WMF respectively [85]. The highest binding energy inhibition constant ki is 36.78, 279.66, 116.92 and 175.03 μm respectively. The protein-ligand interaction binding energy is listed in Table 6. Figs. 13, 13(a), 13(b) and 13(c) shows protein-ligand interaction binding sites. In 4LEB protein docked with 5BRSET and showed two conventional hydrogen bonds such as Lys132 and Cys133 respectively. The titled compound interacted with 4WJY protein and showed two conventional hydrogen bonds named as Gly93 and Glu62. Furthermore, the proteins 8BXA and 2WMF interacted with 5BRSET, the 8BXA is showed one conventional hydrogen bond and 2WMF is showed two conventional hydrogen bonds such as Asn445 and Asp37, Glu7 respectively.

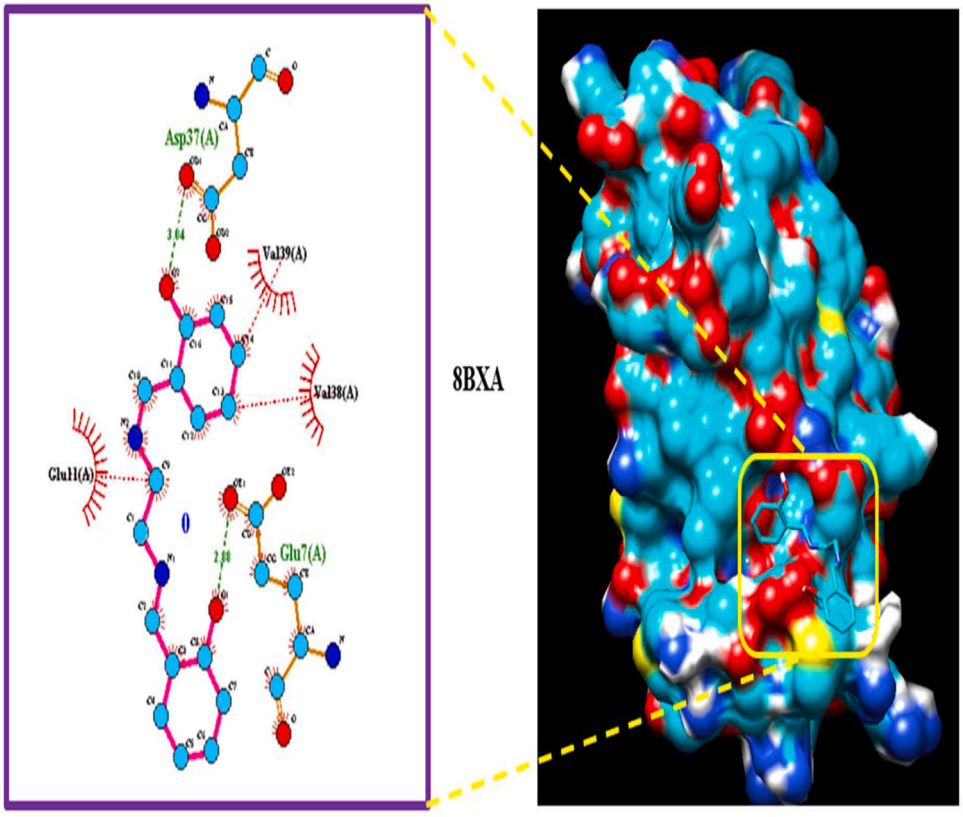

Fig. 13(c). Protein-ligand interaction sites of 5BRSET with 8BXA protein.

Conclusion

The local energy decomposition analysis (LED) calculated final binding energy is −9.19 kcal/mol. The emission (fluorescence) spectrum confirms the wavelength at 512 nm. In UV-visible spectrum show three different wavelength such as 391 nm, 329 nm and 320 nm. The simulated absorption spectrum highest wavelength is 325 nm, which is recorded from water solvent. The titled compound nucleophilic and electrophilic attacking sites confirmed by MEP study. Water solvent showed highest electrostatic potential range, which is −4.881 e^{-2} – 4.881 e^{-2}. In FMO study water solvent have the highest energy gap value (4.33 eV). The localized and delocalized orbitals are confirmed by using topological analysis. The synthesized compound has better antibacterial activity against *E. coli*. The molecular docking study results shows the highest binding affinity score is −5.36 kcal/mol. When compare to other proteins the 8BXA-5BRSET complex have the highest binding affinity score.

CRediT authorship contribution statement

C. Geetha Priya: Conceptualization, Methodology. **B.R. Venkatraman:** Software, Validation. **S. Sowrirajan:** Conceptualization, Methodology, Resources. **N. Elangovan:** Writing – original draft, Data curation, Resources, Writing – review & editing. **Natarajan Arumugam:** Methodology, Resources. **Abdulrahman I. Almansour:** Data curation, Resources. **Sakkarapalayam M. Mahalingam:** Validation.

Declaration of Competing Interest

The authors declare that they have no known competing financial interests or personal relationships that could have appeared to influence the work reported in this paper.

Data availability

Data will be made available on request.

Acknowledgement

The project was funded by Researchers Supporting Project number (RSP2023R231), King Saud University, Riyadh, Saudi Arabia.

Supplementary materials

Supplementary material associated with this article can be found, in the online version, at doi:10.1016/j.chphi.2023.100323.

References

[1] Y. Sert, M. Gümüş, H. Gökce, İ. Kani, İ. Koca, Molecular docking, Hirshfeld surface, structural, spectroscopic, electronic, NLO and thermodynamic analyses on novel hybrid compounds containing pyrazole and coumarin cores, J. Mol. Struct. 1171 (2018) 850–866, https://doi.org/10.1016/j.molstruc.2018.06.069.
[2] H. Gökce, N. Öztürk, Y. Sert, A.S. El-Azab, N.A. AlSaif, A.A.M. Abdel-Aziz, 4-[(1, 3-Dioxoisoindolin-2-yl)methyl]benzenesulfonamide: full structural and spectroscopic characterization and molecular docking with carbonic anhydrase II, ChemistrySelect 3 (2018) 10113–10124, https://doi.org/10.1002/slct.201802484.
[3] M. Gümüş, Ş.N. Babacan, Y. Demir, Y. Sert, İ. Koca, İ. Gülçin, Discovery of sulfadrug–pyrrole conjugates as carbonic anhydrase and acetylcholinesterase inhibitors, Arch. Pharm. (Weinh.). 355 (2022) 1–14, https://doi.org/10.1002/ardp.202100242.
[4] K.J. Rajimon, N. Elangovan, A. Amir, R. Thomas, Schiff bases from chlorine substituted anilines and salicylaldehyde : synthesis, characterization, fluorescence, thermal features, biological studies and electronic structure investigations, J. Mol. Liq. 370 (2023), 121055, https://doi.org/10.1016/j.molliq.2022.121055.
[5] A. Bhardwaj, M. Kumar, S. Garg, D. Kumar, Organotellurium(IV) complexes derived from thiophene based Schiff base 5-methyl-2-thiophene carboxaldehyde: synthesis, spectral characterization, thermal analysis potent antimicrobial and antioxidant activities supported by molecular docking, DFT studies, Inorg. Chem. Commun. 157 (2023), 111332, https://doi.org/10.1016/j.inoche.2023.111332.
[6] Mamta, Subhash, Pinki, A. Chaudhary, In vitro cytotoxicity and antimicrobial evaluation of novel 24–28 membered Schiff base octaazamacrocyclic complexes of

manganese(II): synthesis, characterization, DFT and molecular docking studies, J. Mol. Struct. 1275 (2023), 134667, https://doi.org/10.1016/j.molstruc.2022.134667.
[7] M.S. Begum, D. Das, E. Zangrando, S. Rahman, A. Alodhayb, M.K. Begum, C. M. Sheikh, R. Miyatake, M.B.H. Howlader, M.R. Karim, M.B. Chowdhury, A dithiocarbazate N,S Schiff base ligand with a long alkyl chain: synthesis, characterization, DFT study and antimicrobial activity of its Ni(II) complex, J. Mol. Struct. 1277 (2023), 134808, https://doi.org/10.1016/j.molstruc.2022.134808.
[8] R. Kalarani, M. Sankarganesh, G.G.V. Kumar, M. Kalanithi, Synthesis, spectral, DFT calculation, sensor, antimicrobial and DNA binding studies of Co(II), Cu(II) and Zn (II) metal complexes with 2-amino benzimidazole Schiff base, J. Mol. Struct. 1206 (2020), 127725, https://doi.org/10.1016/j.molstruc.2020.127725.
[9] Shehnaz, W.A. Siddiqui, M.A. Raza, A. Ashraf, M. Ashfaq, M.N. Tahir, S. Niaz, Structure elucidation {single X-ray crystal diffraction studies, Hirshfeld surface analysis, DFT} and antibacterial studies of sulfonamide functionalized Schiff base Copper (II) and Zinc (II) complexes, J. Mol. Struct. (2023), 136603, https://doi.org/10.1016/j.molstruc.2023.136603.
[10] T.S. Ganesan, N. Elangovan, V. Vanmathi, S. Sowrirajan, S. Chandrasekar, K.R. S. Murthy, R. Thomas, Spectroscopic, Computational(DFT), Quantum mechanical studies and protein-ligand interaction of Schiff base 6,6-((1,2-phenylenebis (azaneylylidene))bis(methaneylylidene))bis(2-methoxyphenol) from o-phenylenediamine and 3- methoxysalicylaldehyde, J. Indian Chem. Soc. 99 (2022), 100713, https://doi.org/10.1016/j.jics.2022.100713.
[11] N. Elangovan, B. Gangadharappa, R. Thomas, A. Irfan, Synthesis of a versatile Schiff base 4-((2-hydroxy-3, 5-diiodobenzylidene) amino) benzenesulfonamide from 3, 5-diiodosalicylaldehyde and sulfanilamide, structure, electronic properties, biological activity prediction and experimental antimicrobial propert, J. Mol. Struct. 1250 (2022), 131700.
[12] S.L. Dhonnar, R.A. More, V.A. Adole, B.S. Jagdale, N.V. Sadgir, S.S. Chobe, Synthesis, spectral analysis, antibacterial, antifungal, antioxidant and hemolytic activity studies of some new 2,5-disubstituted-1,3,4-oxadiazoles, J. Mol. Struct. 1253 (2022), 132216, https://doi.org/10.1016/j.molstruc.2021.132216.
[13] G. Rajkumar, R. Sundar, Biogenic one-step synthesis of silver nanoparticles (AgNPs) using an aqueous extract of Persea americana seed: characterization, phytochemical screening, antibacterial, antifungal and antioxidant activities, Inorg. Chem. Commun. 143 (2022), 109817, https://doi.org/10.1016/j.inoche.2022.109817.
[14] B. Essghaier, R. Dridi, A. Arouri, M.F. Zid, Synthesis, structural characterization and prospects for a new tris (5-methylbenzimidazole) tris (oxalato) ferrate(III) trihydrate complex as a promising antibacterial and antifungal agent, Polyhedron 208 (2021), 115420, https://doi.org/10.1016/j.poly.2021.115420.
[15] M.J. Frisch, G.W. Trucks, H.B. Schlegel, G.E. Scuseria, M.A. Robb, J.R. Cheeseman, G. Scalmani, V. Barone, B. Mennucci, G.A. Petersson, H. Nakatsuji, M. Caricato, X. Li, H.P. Hratchian, A.F. Izmaylov, J. Bloino, G. Zheng, J.L. Sonnenberg, M. Hada, M. Ehara, K. Toyota, R. Fukuda, J. Hasegawa, M. Ishida, T. Nakajima, Y. Honda, O. Kitao, H. Nakai, T. Vreven, J.A. Montgomery, J.E. Peralta, F. Ogliaro, M. Bearpark, J.J. Heyd, E. Brothers, K.N. Kudin, V.N. Staroverov, R. Kobayashi, J. Normand, K. Raghavachari, A. Rendell, J.C. Burant, S.S. Iyengar, J. Tomasi, M. Cossi, N. Rega, J.M. Millam, M. Klene, J.E. Knox, J.B. Cross, V. Bakken, C. Adamo, J. Jaramillo, R. Gomperts, R.E. Stratmann, O. Yazyev, A.J. Austin, R. Cammi, C. Pomelli, J.W. Ochterski, R.L. Martin, K. Morokuma, V.G. Zakrzewski, G.A. Voth, P. Salvador, J.J. Dannenberg, S. Dapprich, A.D. Daniels, Farkas, J. B. Foresman, J.V. Ortiz, J. Cioslowski, D.J. Fox, Gaussian 09, Revision B.01, Gaussian 09, Revis. B.01, Gaussian, Inc., Wallingford CT, 2009, pp. 1–20, citeulike-article-id:9096580.
[16] A. Abozeed, M. Sayed, O. Younis, M.S. Tolba, R. Hassanien, A.M. Kamal El-Dean, S. M. Ibrahim, A. Salah, A. Shakir, R. El-Sayed, Y.A. El-Ossaily, A.F. Al-Hossainy, Characterization and optical behavior of a new indole Schiff base using experimental data and TD-DFT/DMOl3 computations, Opt. Mater. (Amst). 131 (2022), 112594, https://doi.org/10.1016/j.optmat.2022.112594.
[17] Ö. Tamer, N. Dege, G. Demirtaş, D. Avcı, Y. Atalay, M. Macit, S. Şahin, Crystal structure and spectroscopic characterization of (E)-2-(((4-bromo-2-(trifluoromethoxy)phenyl)imino)methyl)-4-nitrophenol: a combined experimental and computational study, J. Mol. Struct. 1063 (2014) 295–306, https://doi.org/10.1016/j.molstruc.2014.01.079.
[18] S. Soltani, P. Magri, M. Rogalski, M. Kadri, Charge-transfer complexes of hypoglycemic sulfonamide with π-acceptors: experimental and DFT-TDDFT studies, J. Mol. Struct. 1175 (2019) 105–116, https://doi.org/10.1016/j.molstruc.2018.07.074.
[19] S. Demir, F. Tinmaz, N. Dege, I.O. Ilhan, Vibrational spectroscopic studies, NMR, HOMO–LUMO, NLO and NBO analysis of 1-(2-nitrobenzoyl)-3,5-diphenyl-4,5-dihydro-1H-pyrazole with use X-ray diffractions and DFT calculations, J. Mol. Struct. 1108 (2016) 637–648, https://doi.org/10.1016/j.molstruc.2015.12.057.
[20] F. El Kalai, K. Karrouchi, C. Baydere, S. Daoui, M. Allali, N. Dege, N. Benchat, S. A. Brandán, Synthesis, crystal structure, spectroscopic studies, NBO, AIM and SQMFF calculations of new pyridazinone derivative, J. Mol. Struct. 1223 (2021), 129213, https://doi.org/10.1016/j.molstruc.2020.129213.
[21] T. Lu, F. Chen, Multiwfn: a multifunctional wavefunction analyzer, J. Comput. Chem. 33 (2012) 580–592, https://doi.org/10.1002/jcc.22885.
[22] X. Meng, R. Yang, How formaldehyde affects the thermo-oxidative and photo-oxidative mechanism of polypropylene: a DFT/TD-DFT study, Polym. Degrad. Stab. 205 (2022), 110131, https://doi.org/10.1016/j.polymdegradstab.2022.110131.
[23] D. Parmar, M. Rani, N. Kumar, N. Issaoui, O.M. Al-Dossary, K. Kumari, M. Sahal, L. G. Bousiakoug, Molecular interaction analysis and transport properties of binary liquid mixtures containing 1-Amino-2-propanol and alkyl acetates at T = 298.15–318.15 K: application of Graph theory and DFT studies, J. Saudi Chem. Soc. 27 (2023), 101656, https://doi.org/10.1016/j.jscs.2023.101656.
[24] A.P. Singh Raman, P. Jain, A. Kumar, J. Tomar, N. Kaushik, E.H. Choi, N. K. Kaushik, L. Negadi, P. Singh, Investigate oxoazolidine-2,4-dione based eutectic mixture via DFT calculations and SAR, J. Indian Chem. Soc. 99 (2022), 100570, https://doi.org/10.1016/j.jics.2022.100570.
[25] I. Jomaa, C. Daghar, N. Issaoui, T. Roisnel, H. Marouani, Supramolecular association of (1,4-phenylenedimethanaminium) bis(perchlorate) monohydrate: a combined experimental and theoretical study, J. Mol. Struct. 1272 (2023), 134212, https://doi.org/10.1016/j.molstruc.2022.134212.
[26] H. Yang, B. Xing, J. Zhao, G. Ma, Methoxyl-substituted phosphine ligand properties and a case study of formation adducts to indium(III) bromide by DFT calculations, Polyhedron 225 (2022), 116043, https://doi.org/10.1016/j.poly.2022.116043.
[27] W.B. Schneider, G. Bistoni, M. Sparta, M. Saitow, C. Riplinger, A.A. Auer, F. Neese, Decomposition of intermolecular interaction energies within the local pair natural orbital coupled cluster framework, J. Chem. Theory Comput. 12 (2016) 4778–4792, https://doi.org/10.1021/acs.jctc.6b00523.
[28] A. Jaworski, N. Hedin, Local energy decomposition analysis and molecular properties of encapsulated methane in fullerene (CH4@C60), Phys. Chem. Chem. Phys. 23 (2021) 21554–21567, https://doi.org/10.1039/d1cp02333k.
[29] A. Altun, F. Neese, G. Bistoni, Local energy decomposition analysis of hydrogen-bonded dimers within a domain-based pair natural orbital coupled cluster study, Beilstein J. Org. Chem. 14 (2018) 919–929, https://doi.org/10.3762/BJOC.14.79.
[30] E.M. Nickless, S.E. Holroyd, G. Hamilton, K.C. Gordon, J.J. Wargent, Analytical method development using FTIR-ATR and FT-Raman spectroscopy to assay fructose, sucrose, glucose and dihydroxyacetone, in Leptospermum scoparium nectar, Vib. Spectrosc. 84 (2016) 38–43, https://doi.org/10.1016/j.vibspec.2016.02.011.
[31] M. Faizan, S.A. Bhat, M.J. Alam, Z. Afroz, S. Ahmad, Anharmonic vibrational and electronic spectral study of 2-amino-4-hydroxy-6–methylpyrimidine: a combined experimental (FTIR, FT-Raman, UV–Vis) and theoretical (DFT, MP2) approach, J. Mol. Struct. 1148 (2017) 89–100, https://doi.org/10.1016/j.molstruc.2017.07.007.
[32] P. Manjusha, J. Christian, S. Muthu, B.F. Rizwana, Spectroscopic elucidation (FT-IR, FT-Raman and UV-visible) with NBO, NLO, ELF, LOL, drug likeness and molecular docking analysis on 1- (2- ethylsulfonylethyl) -2-methyl-5-nitro-imidazole : an antiprotozoal agent, Comput. Biol. Chem. 88 (2020), 107330, https://doi.org/10.1016/j.compbiolchem.2020.107330.
[33] M. Kadari, E.H. Belarbi, T. Moumene, S. Bresson, B. Haddad, O. Abbas, B. Khelifa, Comparative study between 1-Propyl-3-methylimidazolium bromide and trimethylene bis-methylimidazolium bromide ionic liquids by FTIR/ATR and FT-RAMAN spectroscopies, J. Mol. Struct. 1143 (2017) 91–99, https://doi.org/10.1016/j.molstruc.2017.04.076.
[34] C.E.S. Nogueira, M.M. de Oliveira, A.M.R. Teixeira, P.N. Bandeira, H.S. dos Santos, A.P. Ayala, B.P. Bezerra, A.C.H. Barreto, P.T.C. Freire, Crystal structure, FT-Raman and FTIR spectra and DFT calculations of chalcone (2E)-1-(4-aminophenyl)-3-(furan-2-yl)prop-2-en-1-one monohydrate, J. Mol. Struct. 1212 (2020), 128141, https://doi.org/10.1016/j.molstruc.2020.128141.
[35] T. Ramya, S. Gunasekaran, G.R. Ramkumaar, Density functional theory, restricted Hartree – Fock simulations and FTIR, FT-Raman and UV–Vis spectroscopic studies on lamotrigine, Spectrochim. Acta Part A Mol. Biomol. Spectrosc. 114 (2013) 277–283, https://doi.org/10.1016/j.saa.2013.05.057.
[36] N. Elangovan, R. Thomas, S. Sowrirajan, Synthesis of Schiff base (E)-4-((2-hydroxy-3,5-diiodobenzylidene)amino)-N-thiazole-2-yl)benzenesulfonamide with antimicrobial potential, structural features, experimental biological screening and quantum mechanical studies, J. Mol. Struct. 1250 (2022), 131762, https://doi.org/10.1016/j.molstruc.2021.131762.
[37] G. J, S. A, A. M, E. N, S. S, S. Manivel, R. Thomas, Synthesis, characterization, computational, excited state properties, wave function and molecular docking studies of (E)-1-(perfluorophenyl)-N-(p-tolyl) methanimine, J. Indian Chem. Soc. (2022), 100785, https://doi.org/10.1016/j.jics.2022.100785.
[38] O.A.A. Ali, N. Elangovan, S.F. Mahmoud, M.S. El-Gendey, H.Z.E. Elbasheer, S. M. El-Bahy, R. Thomas, Synthesis, characterization, vibrational analysis and computational studies of a new Schiff base from pentafluoro benzaldehyde and sulfanilamide, J. Mol. Struct. 1265 (2022), 133445, https://doi.org/10.1016/j.molstruc.2022.133445.
[39] R. Jayachitra, G. Thilagavathi, A. Kanagavalli, N. Elangovan, A. Sirajunnisa, S. Sowrirajan, R. Thomas, Synthesis, computational, electronic spectra, and molecular docking studies of 4-((diphenylmethylene)amino)-N-(pyrimidin-2-yl) benzenesulfonamide, J. Indian Chem. Soc. 100 (2023), 100836, https://doi.org/10.1016/j.jics.2022.100836.
[40] S. Gauthier, A. Porter, S. Achelle, T. Roisnel, V. Dorcet, A. Barsella, N. Le Poul, P. Guevara Level, D. Jacquemin, F. Robin-Le Guen, Mono- and diplatinum polyynediyl complexes as potential push–pull chromophores: synthesis, characterization, TD-dft modeling, and photophysical and NLO properties, Organometallics 37 (2018) 2232–2244, https://doi.org/10.1021/acs.organomet.8b00223.
[41] Y. Oueslati, S. Kansız, A. Valkonen, T. Sahbani, N. Dege, W. Smirani, Synthesis, crystal structure, DFT calculations, Hirshfeld surface, vibrational and optical properties of a novel hybrid non-centrosymmetric material (C10H15N2)2H2P2O7, J. Mol. Struct. 1196 (2019) 499–507, https://doi.org/10.1016/j.molstruc.2019.06.110.
[42] A.A. Kalinin, M.A. Smirnov, L.N. Islamova, G.M. Fazleeva, T.A. Vakhonina, A. I. Levitskaya, O.D. Fominykh, N.V. Ivanova, A.R. Khamatgalimov, I.R. Nizameev, M.Y. Balakina, Synthesis and characterization of new second-order NLO chromophores containing the isomeric indolizine moiety for electro-optical

materials, Dye. Pigment. 147 (2017) 444–454, https://doi.org/10.1016/j.dyepig.2017.08.047.
[43] A.A. Kagilev, V.I. Morozov, E.M. Zueva, Z.N. Gafurov, I.K. Mikhailov, A. O. Kantyukov, I.F. Sakhapov, N.A. Zhukova, M.S. Kadyrova, V.A. Mamedov, D. G. Yakhvarov, Electrochemical behaviour of 2,2′-bibenzimidazoles: voltammetric, in situ UV–vis- and EPR-spectroelectrochemical and computational studies, J. Electroanal. Chem. 921 (2022), 116669, https://doi.org/10.1016/j.jelechem.2022.116669.
[44] S. Genç, N. Dege, A. Çetin, A. Cansız, M. Şekerci, M. Dinçer, 3-(2-Hydro-xy-phenyl)-4-phenyl-1H-1,2,4-triazole-5(4H)-thione, Acta Crystallogr. Sect. E. 60 (2004), https://doi.org/10.1107/S1600536804020367 o1580–o1582.
[45] R. Hsissou, S. Abbout, F. Benhiba, R. Seghiri, Z. Safi, S. Kaya, S. Briche, G. Serdaroğlu, H. Erramli, A. Elbachiri, A. Zarrouk, A. El Harfi, Insight into the corrosion inhibition of novel macromolecular epoxy resin as highly efficient inhibitor for carbon steel in acidic mediums: synthesis, characterization, electrochemical techniques, AFM/UV–Visible and computational investigations, J. Mol. Liq. 337 (2021), 116492, https://doi.org/10.1016/j.molliq.2021.116492.
[46] R M. B, Y.D. Bodke, S.Kumar Jain, L.T. N, S.M. A, Novel isoxazolone based azo dyes: synthesis, characterization, computational, solvatochromic UV–Vis absorption and biological studies, J. Mol. Struct. 1244 (2021), 130933, https://doi.org/10.1016/j.molstruc.2021.130933.
[47] R. Golbedaghi, L.L.G. Justino, F. Ooshall, S. Jamehbozorgi, M. Abdolmaleki, R. Fausto, A new Schiff base ligand as a fluorescence probe for Cu(II) detection in semi-aqueous solution: synthesis, characterization, fluorescence and mechanistic insight, Inorganica Chim. Acta. 528 (2021), 120623, https://doi.org/10.1016/j.ica.2021.120623.
[48] G. Kalaiarasi, M. Ranjani, R. Prabhakaran, P.R. Athira, A. Kosiha, A novel coumarin based probe for Al(III): synthesis, spectral characterization, photophysical properties, DFT calculations and fluorescence cellular bio-imaging, Inorganica Chim. Acta. 535 (2022), 120846, https://doi.org/10.1016/j.ica.2022.120846.
[49] I. Mondal, S. Chatterjee, S. Chattopadhyay, An acetate bridged centrosymmetric zinc(II) complex with a tetradentate reduced Schiff base ligand: synthesis, characterization and ability to sense nitroaromatics by turn off fluorescence response, Polyhedron 190 (2020), 114735, https://doi.org/10.1016/j.poly.2020.114735.
[50] D. Liu, R. Lin, H. Wu, J. Ji, D. Wang, Z. Xue, S. Feng, X. Chen, Green synthesis, characterization of procyanidin-mediated gold nanoparticles and its application in fluorescence detection of prazosin, Microchem. J. 173 (2022), 107045, https://doi.org/10.1016/j.microc.2021.107045.
[51] J. Ebrahimian, M. Khayatkashani, N. Soltani, Q.A. Yousif, M. Salavati-Niasari, Catechin mediated green synthesis of Au nanoparticles: experimental and theoretical approaches to the determination HOMO-LUMO energy gap and reactivity indexes for the (+)-epicatechin (2S, 3S), Arab. J. Chem. 15 (2022), 103758, https://doi.org/10.1016/j.arabjc.2022.103758.
[52] G. Karpagakalyaani, J.D. Magdaline, T. Chithambarathanu, Comparative spectral (FT-IR, FT-Raman, UV) investigations, HOMO–LUMO, NBO and in-silico docking analysis of Nikethamide, niazid and 2-Mercaptonicotinic acid, J. Mol. Struct. 1252 (2022), 132032, https://doi.org/10.1016/j.molstruc.2021.132032.
[53] F.B. A, F. Liakath Ali Khan, S. Muthu, M. Raja, Computational evaluation on molecular structure (Monomer, Dimer), RDG, ELF, electronic (HOMO-LUMO, MEP) properties, and spectroscopic profiling of 8-Quinolinesulfonamide with molecular docking studies, Comput. Theor. Chem. 1198 (2021), 113169, https://doi.org/10.1016/j.comptc.2021.113169.
[54] N. Elangovan, R. Thomas, S. Sowrirajan, A. Irfan, Synthesis, spectral and quantum mechanical studies and molecular docking studies of Schiff base (E)2-hydroxy-5-(((4-(N-pyrimidin-2-yl)sulfamoyl)phenyl)imino)methyl benzoic acid from 5-formyl salicylic acid and sulfadiazine, J. Indian Chem. Soc. 98 (2021), 100144, https://doi.org/10.1016/j.jics.2021.100144.
[55] S. Janeoo, Reenu, A. Saroa, R. Kumar, H. Kaur, Computational investigation of bioactive 2,3-diaryl quinolines using DFT method: FT- IR, NMR spectra, NBO, NLO, HOMO-LUMO transitions, and quantum-chemical properties, J. Mol. Struct. 1253 (2022), 132285, https://doi.org/10.1016/j.molstruc.2021.132285.
[56] B. Ghosh, N. Roy, D. Roy, S. Mandal, S. Ali, P. Bomzan, K. Roy, M.N. Roy, An extensive investigation on supramolecular assembly of a drug (MEP) with βCD for innovative applications, J. Mol. Liq. 344 (2021), 117977, https://doi.org/10.1016/j.molliq.2021.117977.
[57] S. Silvarajoo, U.M. Osman, K.H. Kamarudin, M.H. Razali, H.M. Yusoff, I.U.H. Bhat, M.Z.H. Rozaini, Y. Juahir, Dataset of theoretical molecular electrostatic potential (MEP), Highest occupied molecular orbital-lowest unoccupied molecular orbital (HOMO-LUMO) band gap and experimental cole-cole plot of 4-(ortho-, meta- and para-fluorophenyl)thiosemicarbazide isomers, Data Br. 32 (2020), 106299, https://doi.org/10.1016/j.dib.2020.106299.
[58] N. Elangovan, R. Thomas, S. Sowrirajan, K.P. Manoj, A. Irfan, Synthesis, spectral characterization, electronic structure and biological activity screening of the Schiff base 4-((4-hydroxy-3-methoxy-5-nitrobenzylidene)amino)-n-(pyrimidin-2-yl) benzene sulfonamide from 5-nitrovaniline and sulphadiazene, Polycycl. Aromat. Compd. 0 (2021) 1–18, https://doi.org/10.1080/10406638.2021.1991392.
[59] M.H. Rahuman, S. Muthu, B.R. Raajaraman, M. Raja, H. Umamahesvari, Heliyon Investigations on 2- (4-Cyanophenylamino) acetic acid by FT-IR, FT-Raman, NMR and UV–Vis spectroscopy, DFT (NBO, HOMO-LUMO, MEP and Fukui function) and molecular docking studies, Heliyon 6 (2020) e04976, https://doi.org/10.1016/j.heliyon.2020.e04976.
[60] E.A. Soares, C. Téllez, S.A. Fortes, A. Coelho, O. Versiane, G.B. Ferreira, M. A. Mondragón, C.A. TéllezS, Fourier transform infrared and Raman spectra of the complex cation diethyldithiocarbamate Cr(III) Di-hydrate, [Cr(DDTC)2(OH2)2]+. UV–Vis spectrum, DFT:B3LYP/6-311G(d, p) structural determination, vibrational and natural bond orbital analysis, J. Mol. Struct. 1256 (2022), 132555, https://doi.org/10.1016/j.molstruc.2022.132555.
[61] C.A. Téllez S, A.C. Costa, M.A. Mondragón, G.B. Ferreira, O. Versiane, J.L. Rangel, G.M. Lima, A.A. Martin, Molecular structure, natural bond analysis, vibrational and electronic spectra, surface enhanced Raman scattering and Mulliken atomic charges of the normal modes of [Mn(DDTC)2] complex, Spectrochim. Acta Part A Mol. Biomol. Spectrosc. 169 (2016) 95–107, https://doi.org/10.1016/j.saa.2016.06.018.
[62] N. Elangovan, S. Sowrirajan, K.P. Manoj, A.M. Kumar, Synthesis, structural investigation, computational study, antimicrobial activity and molecular docking studies of novel synthesized (E)-4-((pyridine-4-ylmethylene)amino)-N-(pyrimidin-2-yl)benzenesulfonamide from pyridine-4-carboxaldehyde and sulfadiazine, J. Mol. Struct. 1241 (2021), 130544, https://doi.org/10.1016/j.molstruc.2021.130544.
[63] M. Alam, S. Park, Molecular structure, spectral studies, NBO, HOMO–LUMO profile, MEP and Mulliken analysis of 3β,6β-dichloro-5α-hydroxy-5α–cholestane, J. Mol. Struct. 1159 (2018) 33–45, https://doi.org/10.1016/j.molstruc.2018.01.043.
[64] M. Arivazhagan, R. Kavitha, Molecular structure, vibrational spectroscopic, NBO, HOMO–LUMO and Mulliken analysis of 4-methyl-3-nitro benzyl chloride, J. Mol. Struct. 1011 (2012) 111–120, https://doi.org/10.1016/j.molstruc.2011.12.006.
[65] C.A. Téllez Soto, A.C. Costa, J.M. Ramos, O. Versiane, G.F. Ondar, G.B. Ferreira, P. P. Fávero, J.L. Rangel, L. Raniero, G. Bueno Costa, G.G.A. Bussi, A.A. Martin, Surface enhanced Raman scattering, electronic spectrum and Mulliken charge distribution in the normal modes of bis(diethyldithiocarbamate)zinc(II) complex, Spectrochim. Acta Part A Mol. Biomol. Spectrosc. 110 (2013) 443–449, https://doi.org/10.1016/j.saa.2013.03.039.
[66] A.S. Kazachenko, N. Issaoui, A. Sagaama, Y.N. Malyar, O. Al-Dossary, L. G. Bousiakou, A.S. Kazachenko, A.V. Miroshnokova, Z. Xiang, Hydrogen bonds interactions in biuret-water clusters: FTIR, X-ray diffraction, AIM, DFT, RDG, ELF, NLO analysis, J. King Saud Univ. - Sci. 34 (2022), 102350, https://doi.org/10.1016/j.jksus.2022.102350.
[67] C.A. Téllez Soto, A.C. Costa, J.M. Ramos, L.S. Vieira, N.C.V Rost, O. Versiane, J. L. Rangel, M.A. Mondragón, L. Raniero, A.A. Martin, Surface enhanced Raman scattering, electronic spectrum, natural bond orbital, and mulliken charge distribution in the normal modes of diethyldithiocarbamate copper (II) complex, [Cu(DDTC)2], Spectrochim. Acta Part A Mol. Biomol. Spectrosc. 116 (2013) 546–555, https://doi.org/10.1016/j.saa.2013.07.083.
[68] M. Aarjane, S. Slassi, A. Ghaleb, A. Amine, Synthesis, spectroscopic characterization (FT-IR, NMR) and DFT computational studies of new isoxazoline derived from acridone, J. Mol. Struct. 1231 (2021), 129921, https://doi.org/10.1016/j.molstruc.2021.129921.
[69] M. P, V. Balraj, G. Vinitha, R. V, Synthesis, structural-spectral characterization and theoretical studies of Pyridinium-4-carbohydrazide 2,4,6-trinitrophenolate, J. Mol. Struct. 1262 (2022), 132779, https://doi.org/10.1016/j.molstruc.2022.132779.
[70] A. Ramalingam, S. Sambandam, M. Medimagh, O. Al-Dossary, N. Issaoui, M. J. Wojcik, Study of a new piperidone as an anti-Alzheimer agent: molecular docking, electronic and intermolecular interaction investigations by DFT method, J. King Saud Univ. - Sci. 33 (2021), 101632, https://doi.org/10.1016/j.jksus.2021.101632.
[71] C.D. Vincy, J.D.D. Tarika, X.D.D. Dexlin, A. Rathika, T.J. Beaula, Exploring the antibacterial activity of 1, 2 diaminoethane hexanedionic acid by spectroscopic, electronic, ELF, LOL, RDG analysis and molecular docking studies using DFT method, J. Mol. Struct. 1247 (2022), 131388, https://doi.org/10.1016/j.molstruc.2021.131388.
[72] A. Sagaama, N. Issaoui, O. Al-Dossary, A.S. Kazachenko, M.J. Wojcik, Non covalent interactions and molecular docking studies on morphine compound, J. King Saud Univ. - Sci. 33 (2021), 101606, https://doi.org/10.1016/j.jksus.2021.101606.
[73] R. Sukanya, D. Aruldhas, I.H. Joe, S. Balachandran, Spectroscopic and quantum chemical computation on molecular structure, AIM, ELF, RDG, NCI, and NLO activity of 4-VINYL benzoic acid: a DFT approach, J. Mol. Struct. 1253 (2022), 132273, https://doi.org/10.1016/j.molstruc.2021.132273.
[74] K. Arulaabaranam, S. Muthu, G. Mani, A.S. Ben Geoffrey, Speculative assessment, molecular composition, PDOS, topology exploration (ELF, LOL, RDG), ligand-protein interactions, on 5-bromo-3-nitropyridine-2-carbonitrile, Heliyon 7 (2021) e07061, https://doi.org/10.1016/j.heliyon.2021.e07061.
[75] F. Gulbagca, S. Ozdemir, M. Gulcan, F. Sen, Synthesis and characterization of Rosa canina-mediated biogenic silver nanoparticles for anti-oxidant, antibacterial, antifungal, and DNA cleavage activities, Heliyon 5 (2019) e02980, https://doi.org/10.1016/j.heliyon.2019.e02980.
[76] S. Zheng, W. Wu, Q. Jiang, C. Lin, Y. Fang, H. Dai, B. Tang, Y. Tan, Synthesis of novel naphthalene-chimonanthine scaffolds hybrids with potent antibacterial or antifungal activity, Nat. Prod. Res. (2022), https://doi.org/10.1080/14786419.2022.2067851.
[77] S.G. Aydinli, Y. Ozdamar, C. Sayil, N. Gulsah Deniz, M. Stasevych, V. Zvarych, O. Komarovska-Porokhnyavets, V. Novikov, Synthesis, characterization and investigation of antibacterial and antifungal activities of novel 1,3-butadiene compounds, Synth. Commun. 50 (2020) 3234–3244, https://doi.org/10.1080/00397911.2020.1799010.
[78] K.M. PrabhuKumar, C.E. Satheesh, P. RaghavendraKumar, M.N.S. Kumar, K. Lingaraju, P.A. Suchetan, H. Rajanaika, Synthesis, characterization, antibacterial, antifungal and antithrombotic activity studies of new chiral selenated Schiff bases and their Pd complexes, J. Mol. Struct. 1264 (2022) 133172, https://doi.org/10.1016/j.molstruc.2022.133172.
[79] Z.T. Omar (Al-Ahdal), S. Jadhav, S. Shejul, P. Chavan, R. Pathrikar, M. Rai, Synthesis, magnetic moment, antibacterial, and antifungal studies of INH

incorporating Schiff base metal complexes, Polycycl. Aromat. Compd. (2022), https://doi.org/10.1080/10406638.2022.2077776.
[80] D. Rajaraman, L.A. Anthony, P. Nethaji, R. Vallangi, One-pot synthesis, NMR, quantum chemical approach, molecular docking studies, drug-likeness and in-silico ADMET prediction of novel 1-(2,3-dihydrobenzo[b][1,4]dioxin-6-yl)-2-(furan-2-yl)-4,5-diphenyl-1H-imidazole derivatives, J. Mol. Struct. 1273 (2023), 134314, https://doi.org/10.1016/j.molstruc.2022.134314.
[81] N. Issaoui, H. Ghalla, F. Bardak, M. Karabacak, N. Aouled Dlala, H.T. Flakus, B. Oujia, Combined experimental and theoretical studies on the molecular structures, spectroscopy, and inhibitor activity of 3-(2-thienyl)acrylic acid through AIM, NBO,FT-IR, FT-Raman, UV and HOMO-LUMO analyses, and molecular docking, J. Mol. Struct. 1130 (2017) 659–668, https://doi.org/10.1016/j.molstruc.2016.11.019.
[82] G. Thilagavathi, R. Jayachitra, A. Kanagavalli, N. Elangovan, A. Sirajunnisa, S. Sowrirajan, R. Thomas, Journal of the Indian chemical society synthesis, computational, molecular docking studies and photophysical amino) benzenesulfonamide, J. Indian Chem. Soc. 100 (2023), 100835, https://doi.org/10.1016/j.jics.2022.100835.
[83] S.R. Begum, D.J. Rao, K.V.R. Rao, Y. Ramakrishna, N. Elangovan, R. Thomas, Quantum mechanical studies of 5-amino-2-(6-(2-hydroxyethyl)-3-oxononyl) cyclohex-2-enone isolated from a marine algae, Vietnam J. Chem. 60 (2022) 362–375, https://doi.org/10.1002/vjch.202100159.
[84] S. Manivel, B.S. Gangadharappa, N. Elangovan, R. Thomas, O.A. Abu Ali, D. I. Saleh, Schiff base (Z)-4-((furan-2-ylmethylene)amino) benzenesulfonamide: synthesis, solvent interactions through hydrogen bond, structural and spectral properties, quantum chemical modeling and biological studies, J. Mol. Liq. 350 (2022), 118531, https://doi.org/10.1016/j.molliq.2022.118531.
[85] F. Hammami, N. Issaoui, S. Nasr, Investigation of hydrogen bonded structure of urea-water mixtures through Infra-red spectroscopy and non-covalent interaction (NCI) theoretical approach, Comput. Theor. Chem. 1199 (2021), 113218, https://doi.org/10.1016/j.comptc.2021.113218.